Review Article

Chenhao Cong[#], Xinlin Li[#], Wei Xiao, Junru Li, Mingliang Jin*, Se Hyun Kim*, and Pengfei Zhang*

Electrohydrodynamic printing for demanding devices: A review of processing and applications

https://doi.org/10.1515/ntrev-2022-0498 received October 27, 2021; accepted November 1, 2022

Abstract: Electrohydrodynamic (EHD) printing is a cutting-edge micro/nano manufacturing technology for flexible substrates. Generally, EHD printing uses an electric field to drive droplet jet printing, which has characteristics of low cost, simple structure, and high precision. According to the research status of EHD printing at home and abroad, this article mainly focuses on the processing and applications of demanding devices by EHD printing, as well as the influence of associated-processing parameters, with regard to the breakthrough of different kinds of electronic inks developed in recent 5 years. Upon the understanding of the challenges and opportunities from the point of view of engineering applications, optimization strategies for ink selection are put forward for driving EHD printing in various fields of transistors, sensors, biomedicine, and electroluminescent devices.

Keywords: electrohydrodynamic jet printing, mechanism, ink material, transistors, applications

Chenhao Cong, Xinlin Li, Junru Li: College of Mechanical and Electrical Engineering, Qingdao University, Qingdao 266071, China Wei Xiao: School of Electronic Engineering, Shandong University of Technology, Zibo 255000, China

1 Introduction

Nowadays, the flexible electronic industry is booming in biomedical and wearable devices, flexible electronic devices, and other fields [1-3]. As pointed out by Wei Huang, flexible electronics will profoundly change the mode of production, way of life, and way of thinking in the life of humans. Electrohydrodynamic (EHD) printing is one of the cutting-edge technologies for manufacturing key components of demanding devices, such as micro/ nano structures and devices. Generally, during the EHD printing process, synthesized electronic ink is transferred to a flexible substrate such as glass, polymer film, silicon substrate, or paper. The EHD printing is a greatly facile technology for demanding devices when compared with any traditional electronic device manufacturing technology, especially, the EHD has low energy consumption and waste emission [4-6]. Figure 1 demonstrates some examples of devices manufactured by traditional and EHD technology. Compared with the conventional photolithography, EHD printing of gold nanopillars with up to 50 nm lateral resolution and aspect ratio higher than 17 demonstrates advantages for stacking from 2D structures to high-precision 3D structures [7]. Its ability to deposit a wide range of inks using solution engineering and without the involvement of mask plates, especially reducing the operation of harsh environments such as photoresist removal by developers, has enabled its broad application prospects in the field of biomaterials to maintain cell activity. However, an important area of continued interest in EHD printing is how to improve the relatively low process throughput compared to the large area manufacturing of photolithography. Two important ways to improve process throughput are to increase the print frequency and to increase the number of nozzles. Chen et al. utilized twotube glass nanoparticles to parallelize nano-drop spraying for a dual 3D nano-printing process [8]. And electric field distribution calculations were made for three and four nozzles to extend to multi-tube nozzle array applications, laying the foundation for commercial use of up to seventube glass capillaries.

[#] These authors contributed equally to this work and should be considered first co-authors.

^{*} Corresponding author: Mingliang Jin, Institute of Translational Medicine, The Affiliated Hospital of Qingdao University, Qingdao 266071, China; Institute for Future Automation School of Qingdao University, Qingdao 266071, China, e-mail: jinmingliang@qdu.edu.cn * Corresponding author: Se Hyun Kim, Division of Chemical

Engineering, Konkuk University, Seoul 05029, Republic of Korea, e-mail: shkimnano@gmail.com

^{*} Corresponding author: Pengfei Zhang, College of Mechanical and Electrical Engineering, Qingdao University, Qingdao 266071, China, e-mail: pzhang@qdu.edu.cn

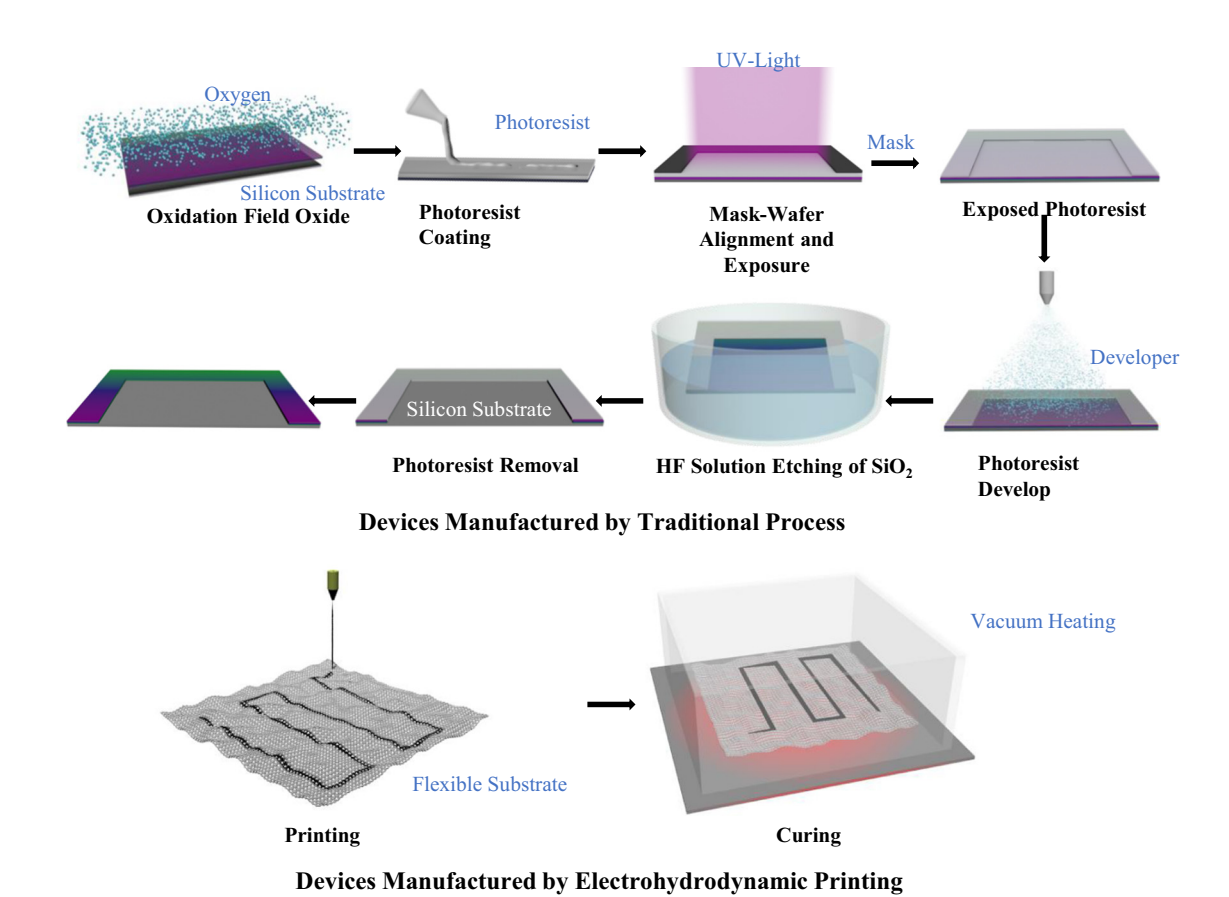


Figure 1: Demonstrations of devices manufactured by traditional process and printing electronic process.

The history and evolution of EHD printing techniques have been examined in a number of published reviews, patents, and books [9-17]. Pioneer work mainly focused on the inclusive concept in working principle of EHD printing, the influence of parameters, ink materials, and applications. The original use of electrostatic fields for electronic printing was introduced by Sir William Thomson in 1876 with the siphon recorder for receiving signals through more or less long cables, a tool for printing telegraphic messages on paper [18]. In the 1950s, electrospray was used in nuclear physics to deposit a thin layer of radioactive material [19]. And then in 1964 , Taylor determined the shape of the cone formed by a fluid at the tip of a capillary in an electric field [20]. At the same year (1964), Sweet developed a high-speed inkjet recorder using an electric field between a charged droplet and an external electrode [21], which Lewis and Brown extended to digital printing in 1967 [22]. After that, a large number of improvements and achievements emerged in the two categories of on-demand printing using electric signals to control the injection of individual ink droplets and continuous printing using electric field force driven printing formed under continuous high pressure [23-26]. In 2007, Park et al. used cone jet mode to print electrodes, increasing the resolution of printed patterns to 10 µm [27]. And they found that the EHD has numerous advantages of great material compatibility, low cost, simple structure, and high resolution. Since then, EHD printing has been applied for jetting high-resolution nanofibers on specific substrates to make stretchable/flexible electronic devices [28]. Liashenko and coworkers printed 3D objects with sub-micron characteristics by electrostatically deflecting jets, with very small radii of curvature by stacking nanofibers layer by layer at frequencies of up to 2,000 Hz [29]. Su and coworkers used a 4 µm radius of curvature (ROC) microtip to obtain nanofibers with a diameter of 30 nm and a necking ratio of ~266:1 [30]. From above discussion, it clearly seems that EHD printing is a high-resolution printing method with ability to manufacture demanding devices at nanoscales. There is no doubt that the previous endeavors have greatly advanced understanding of the EHD printing, or at least created new knowledge on what-to-do and how-to-do when implementing EHD printing for demanding devices. However, due to the fast development in this emerging field, there is a need to review these new developments within the framework of EHD printing for demanding devices.

In this review, we discuss the potential challenges and opportunities from the point of view of engineering applications. It aims at providing an overview of the latest developments in EHD printing technology from the perspective of printing and manufacturing processes. Section 2 analyses the challenges faced by EHD printing process. Section 3 combines breakthroughs in EHD inks developed in recent 5 years, for the sake of optimizing strategies for ink selection. Section 4 summarizes an overview of breakthrough applications by EHD printing in different fields in the last 5 years. The final section concludes the study as well as provides an outlook on the future of the field.

2 Challenges in EHD printing

2.1 Regulations of EHD printing

Among printing electronic technologies, EHD printing is one of the most popular methods to fabricate micro and/or nano-flexible electronic devices in recent years [31]. Usually, EHD printing consists of a high-voltage power supply, a high-speed camera, and an air pump connected to a printing table.

During EHD printing process, high voltage is applied between the nozzle and substrate, while the nozzle is connected with the positive pole of the high voltage power supply. When the nozzle moves to the negative direction of the *Z*-axis, the vertical distance between the nozzle and substrate narrows down, resulting in electrostatic induction, which in turn causes the surface of the substrate to rearrange into negative charges [32]. Meanwhile, a backpressure valve controls pressure from an air pump in order

to squeeze printing ink into a nozzle. The formed high-voltage electric field polarizes droplets when ink comes out from the nozzle. At the same time, the meniscus transforms into a stable cone (*i.e.*, Taylor cone) attributed to the coupling effect between the gravity, viscous force, liquid surface tension, and electric field force. And the positively charged ink at the tip of Taylor cone would be sprayed to form a very fine jet (*i.e.*, cone jet) if the electric field force overcomes the ink's surface tension, as shown in Figure 2 [33–35]. As pointed out by An *et al.* [36], the diameter of an EHD jet is typically 0.01–0.2 times the diameter of the nozzle, which can achieve submicron resolution accuracy and thus enable high-resolution inkjet printing.

It is worth pointing out the difference between EHD printing and traditional dispenser printing. Traditional dispense printing uses pressure to "push" ink out of a nozzle. The diameter of the ink is usually larger than that of the nozzle because of the extrusion swelling. While the EHD printing uses electric field force to "pull" ink out of a nozzle, forming a cone jet. The diameter of the ink is smaller that of the nozzle. It even could be tuned down to a submicron scale, as shown in Figure 3. The EHD printing technology is suitable for most functional material inks because of its wide application range of viscosity [37–39].

EHD printing does not require the assistance of high-cost and sophisticated printing systems. But there are several types of working modes according to their working conditions. Generally, they are categorized into three modes, such as micro-jet printing, electrospinning, and electrospray, as shown in Figure 4. The micro-jet printing is used for producing nanoscale jets or droplets [40]. Electrospinning is for producing micro/nano fibers, having a large application in the textile field [41]. And the electrospray is for producing membranes or thin films [42]. The parameter

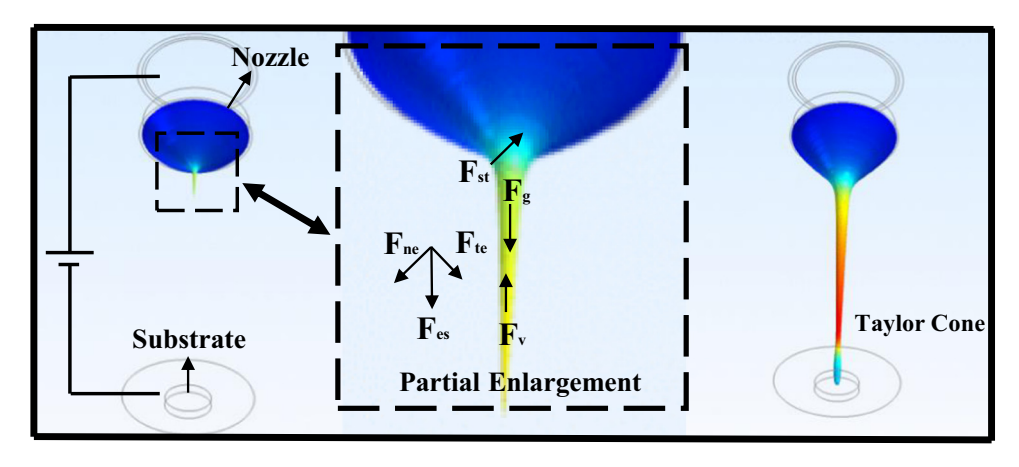


Figure 2: Mechanism of EHD printing.

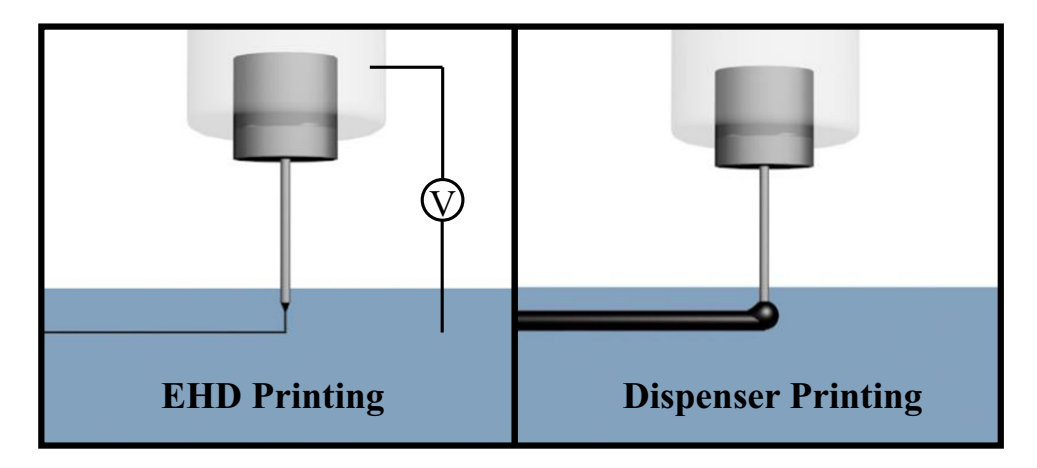


Figure 3: Comparison of EHD printing and traditional dispense printing process principles.

ranges of the three modes of EHD inkjet printing are summarized in Table 1. But there are many factors that affect the stability of EHD printing, such as working distance [43], voltage [44], flow rate [45], printing speed [46], mass fraction [47], and so on.

From Table 1 it can be seen that the working voltage and working distance increase from micro-jet printing to electrospinning and electrospray. The work distance of micro-jet printing is comparatively the smallest. The distance between a nozzle and a base plate is within 1 mm. Therefore, the interference from the air is small, and the accuracy of the printed pattern is high [48]. Hongbo and others found that the process had the phenomenon of automatic calibration in the printing process [49]. When

the nozzle deviates due to the influence of the mechanical precision of the equipment, the droplets still deposit on the surface of the printed solid structure. This is because, despite the nozzle position offset, the entity has a certain height relative to the print substrate, when the nozzle and the surface of the entity are between the strongest electrostatic induction, this makes micro-droplets by the electric field force biased towards the entity spray so that the printing accuracy can be improved.

According to scaling laws, the electric force is quite ineffective when the work distance is in the range above a few millimeters, but it becomes effective when the distance is on a micron scale. The variation in voltage has a large effect on the volume of a droplet jet, the stability of

Working Mode Micro-jet printing Electrospinning Electrospray

Figure 4: Three working modes of EHD printing.

Table 1: Comparison of three EHD printing modes

EHD print	Working mode	Voltage (kV)	Distance (mm)	Solvent	Pattern
Micro-jet printing	Cone-jet, droplet mode	0.5-3	0.1–1	Polymers, nanoparticles	Point, discrete line
Electro-spinning	Cone-jet, multiple modes	1-10	10–50	Polymers, nanoparticles	Continuous ink
Electro-spray	Cone-jet, multiple modes	15-30	100–250	Almost all materials	Film

a cone jet, and the working mode of EHD printing. At the same time, it needs to cooperate with the moving speed of the worktable, while the other two parameters are coupled with each other. It is well-known that continuous inkjet and drop-on-demand inkjet are two main types of inkjet printing [50].

2.2 Challenges in micro-jet printing

2.2.1 Voltage control mode

Although there are various voltage control modes, the principle of printing is more or less the same. Operating at a constant voltage is the most basic mode. Usually, a controlled DC power supply is connected with the nozzle to generate a constant electric field force, called constant voltage mode. Parameters (such as voltage and flow rate) are adjusted so that a stable cone jet can be formed at a nozzle. When the flow rate is less than a critical value (i.e., a minimum value Q_{\min}), it

will not be able to obtain a stable cone jet no matter how voltage is adjusted [51–53]. The effect of voltage on a cone jet is illustrated in Figure 5. The liquid surface is spherical when the voltage is 1.0 kV. Along with the increase in voltage, the curved liquid surface changes from elongated ellipsoidal to pulsating cone tip, pulsating Taylor cone, and stable Taylor cone [54]. Wang and coworkers conducted a study on the formation of continuous cone jets using EHD printing to obtain micro-dripping, spindle, multi-spindle, instantaneous cone-jet, stable cone-jet, and unstable cone-jet [55].

A stable Taylor cone-jet is a result of the coupling of various parameters, such as the surface tension of a liquid, the viscous force of a droplet, the gravity of a droplet itself, and applied electric field force. Generally speaking, the force acting on the Taylor cone has to satisfy the Navier–Stokes (*i.e.*, N–S) equation, explained by equation (1) [56]. Besides, the bottom end of a Taylor cone will rupture once the applied voltage continues to increase until the threshold of the combined force is achieved, leading to the ejecting of a droplet [57].

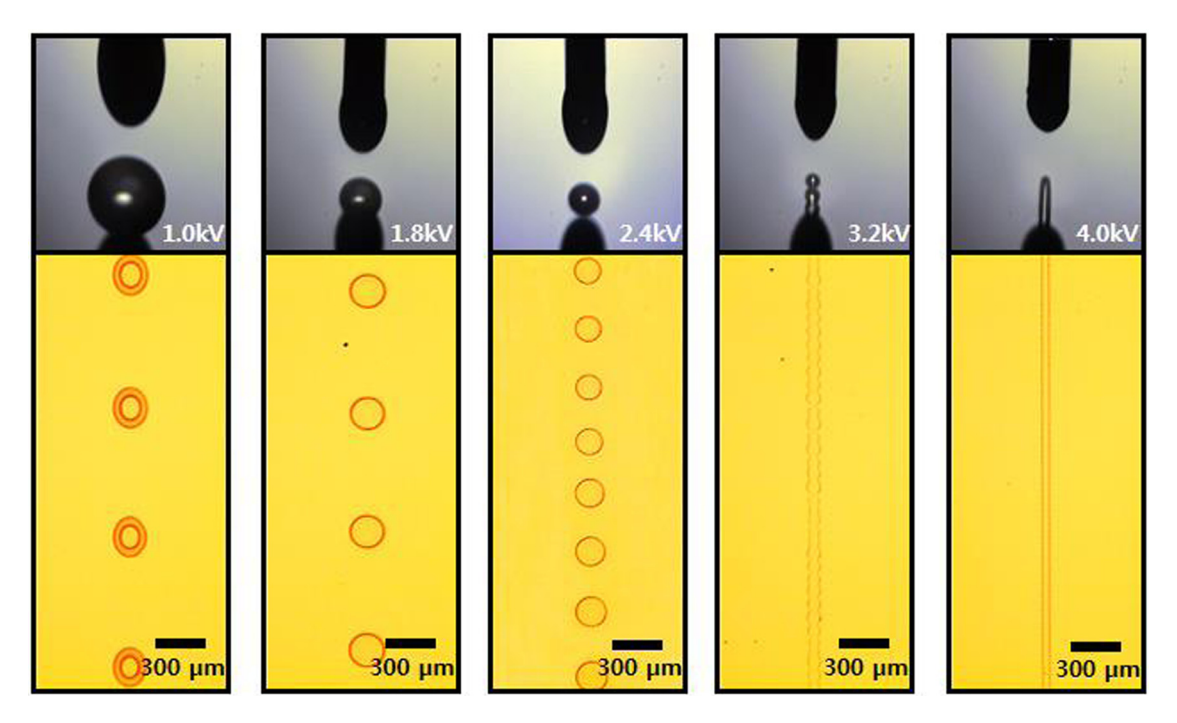


Figure 5: The formation process of continuous cone-jet with the increase in voltages.

$$\rho \left(\frac{\partial u}{\partial t} + u \cdot \nabla u \right) = -\nabla p + F_{\rm v} + F_{\rm es} + F_{\rm st} + F_{\rm g}, \tag{1}$$

where ρ is the charge density of the material; p is pressure; μ is the fluid velocity; $F_{\rm v}$ is the viscous force; $F_{\rm es}$ is the electric field force; $F_{\rm st}$ is the surface tension; and $F_{\rm g}$ is the gravity. It can be concluded that the breakthrough of the bottom of Taylor cone is closely related to the surface tension, charge density, viscosity, and other parameters of the E-ink [58].

It is always a challenge to use conductive materials under the constant voltage mode. This is because the applied voltage will cause an accumulation in an internal charge of the e-ink, which in turn results in an E-ink disorder and even failure of a printed pattern. Thus, how to form a stable Taylor cone becomes an issue when using conductive materials. Some solutions have been proposed to address it [59–61]. For example, regulating the voltage and flow rate in an operating mode of DC voltage is a promising solution among them.

2.2.2 Pulse frequency

The previous section describes the effect of DC voltage mode on EHD printing process and its outcomes. In practice, the constant voltage mode suffers from the problem of instability during printing, making it difficult to achieve high precision on-demand printing. Alternatively, high-voltage pulse printing is used for the sake of solving problems of instability during printing. In this case, a controlled pulse voltage is applied to form an intermittent electric field force. In recent years, pulsed electrojet printing has found a wide range of applications in the fabrication of micro and nano structures [62–64]. In the pulse high-pressure control mode, the printing time is tuned by adjusting the pulse width, thus reducing the flow to achieve a more accurate on-demand printing.

In order to avoid drawbacks resulting from DC constant voltage mode, Fujii and coworkers first tried EHD printing by applying a high voltage pulse at the nozzle to realize an on-demand printing [65]. Subsequently, many researchers started investigations of DC pulse-controlled printing. Wang and coworkers conducted an investigation using a control mode of high-voltage pulses [66]. In their studies, they found that the printing process underwent droop expansion with multiple droop pulsations before jetting at low potentials, but a stable cone-shaped jet was formed at applied pulse voltages and high potentials. It was verified that the droplet deposition frequency was equal to the pulse voltage frequency.

Pulse frequency plays a key role in EHD printing. For example, the pulse frequency directly determines the

time and frequency of the electric field force applied to the nozzle droplets, thus directly affecting the pattern forming accuracy of EHD printing. As mentioned earlier, the liquid surface is deformed into a Taylor cone and undergoes a transition from a charged droplet to a conical jet under an applied pulse voltage. The conical jet pulsates due to an imbalance between the liquid's imprint rate and flow rate [67]. Juraschek and Rollgen categorized the pulsation frequency into low frequency (~10 Hz) and high frequency (~1 kHz) modes. Low-frequency pulsations are generated by imbalances throughout the cone, while highfrequency pulsations occur at the apex of the cone [68]. Different types of pulsations are caused by losing in a liquid jet print and the imbalance created by a difference in the supply of flow to the liquid cone in different areas. After observation of low-frequency pulsations, Kim and coworkers found that the jet frequency was not always linearly related to the voltage frequency [69].

The feeding rate of a droplet is controlled by a backpressure valve in the EHD printing system. The coupling effect between the feeding rate and pulse frequency is greatly critical in determining the shape of a Taylor cone. During the jetting process, the ink meniscus at the tip of the nozzle expands from spherical to conical in the presence of an electric field, and then periodically contracts to spherical. A complete cycle can be divided into four stages, which are liquid accumulation, cone formation, droplet ejection, and relaxation in the accumulation stage. When the ink forms undropped droplets at the tip of the nozzle, its surface tension dominates [70]. Specifically, if the feeding rate of liquid is less than the discharge rate of liquid during the injection process, the entire cone volume will shrink due to rapid injection. When the droplet shrinks to another critical volume, the jet may stop before the pulse closes. As a result, the droplet's ROC would be larger than the critical ROC. After a pulse sequence, the cone volume is small and the ROC at the vertex is large. The cone volume would increase as the pulse sequence continues. But the increase would be ceased once the radius of the liquid surface curvature reduces down to a critical value below Maxwell's stress (i.e., outward electrostatic pressure). At this point, the electric field force exceeds the droplet surface tension, leading to the rupture and ejection of a droplet, as illustrated in Figure 6.

Xu and coworkers carried out a study on the injection frequency under low-frequency pulsation mode and found that the ratio of injection frequency to voltage frequency was 1:N, which is called 1/N rule [71]. The relationship between the jet frequency f, the voltage potential V, and the working height h was proposed by Choi as [72]

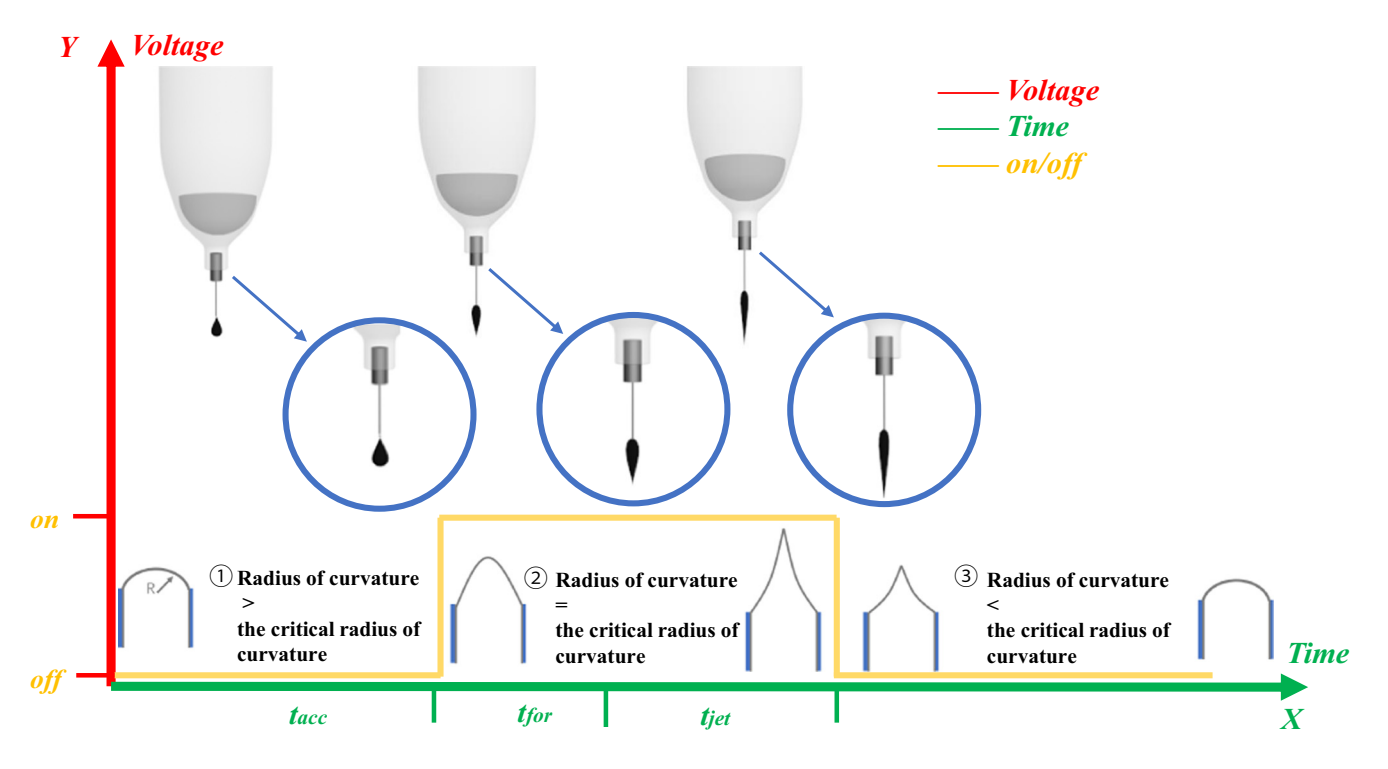


Figure 6: The relationship between the ROC and shape of the Taylor cone within a pulse period.

$$f = K \left(\frac{V}{h}\right)^{2/3},\tag{2}$$

where *K* is a proportionality constant that depends on the viscosity of the ink, the nozzle diameter, the applied backpressure, and the dielectric constant of the space. For a fixed voltage potential, the electric field diminishes significantly as the tip and substrate move away from each other.

2.2.3 Pulse width

The pulse width is a measure of the elapsed time between the leading and trailing edges of a single pulse of EHD supply energy. At low pulse frequency, with the increase in pulse width, droplets at a nozzle will go through a sequence of stages chronologically from unstable injection to stable single injection, unstable secondary injection, and stable secondary injection. Usually, when the pulse voltage frequency is fixed, the frequency of printing will be less than the pulse voltage frequency if the pulse width is not able to support the formation of a complete droplet, which will result in non-uniform droplet diameters. But the droplet diameter will become uniform if the pulse width is sufficient to help the formation of a complete droplet, as shown in Figure 7 [73]. It is worth

noting that the diameter of the printed droplet does not vary with pulse width, but it decreases with increasing pulse voltage frequency.

The duty cycle is the ratio of energizing time relative to total time within a pulse cycle. And it is the ratio of the pulse width to the entire pulse period. The duty cycle plays an important role in affecting the quality and accuracy of a print pattern [74–76]. This is because the pulse voltage action time within a single pulse cycle is determined by the duty cycle, wherein the size affects the state of electric field injection if pulse frequencies are the same. Mishra and coworkers measured the frequency of printed droplets by means of substrate-side current measurement (SSCM) and nozzle-side measurement (NSM) [77]. This is because a small current would be drawn to neutralize an imbalance in a charged fluid at the meniscus when the charged droplet is released from a nozzle. The substrate-side measurement is to measure the current dissipated through a substrate to the ground when a charged droplet arrives at a conductive substrate. The NSM is to measure the time of a droplet when released from a nozzle. In their study, the volume and spacing of droplets were controlled by adjusting pulse width and pulse frequency to obtain the relationship between surface droplet diameter and pulse width. They pointed out that droplet spacing on the substrate can be directly controlled by the duty cycle.

3312 — Chenhao Cong et al. DE GRUYTER

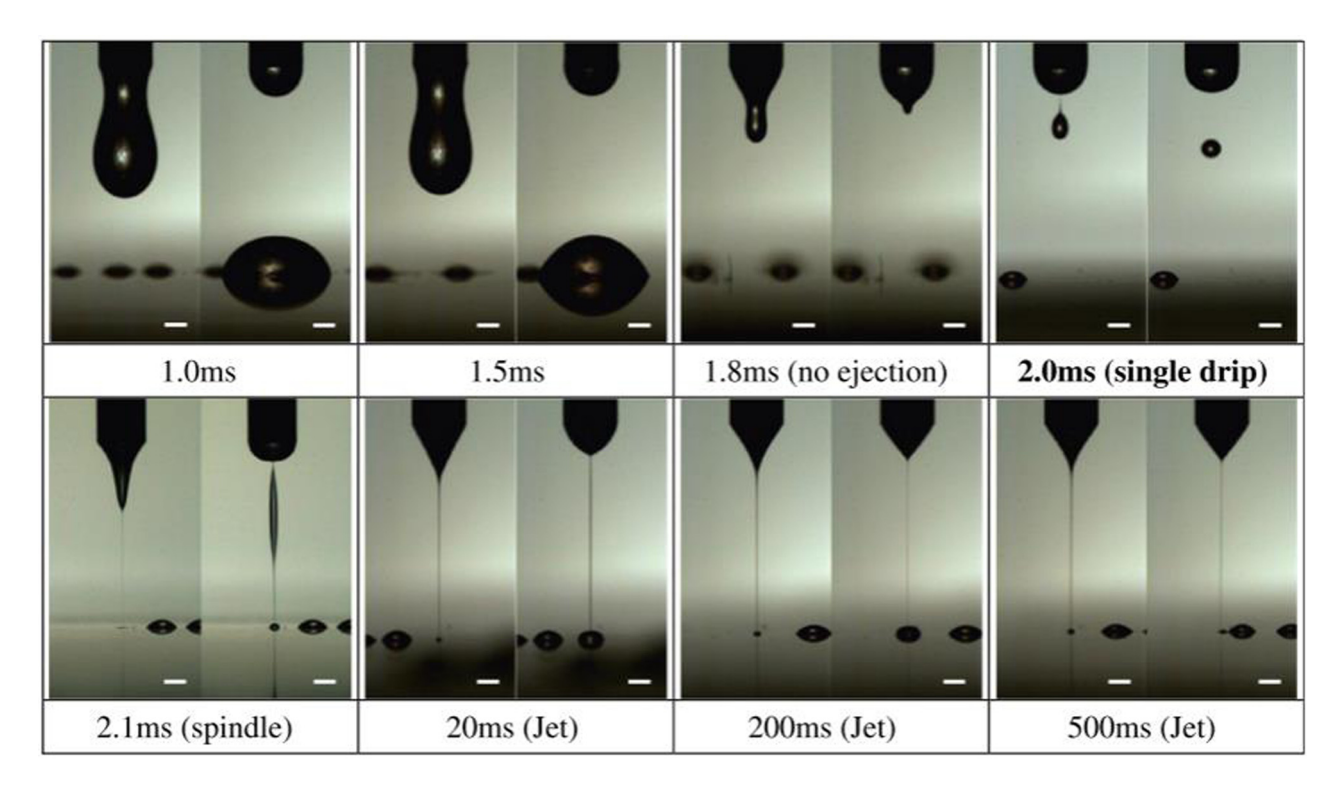


Figure 7: The effect of the pulse width on the micro-jet and drop mode (reproduced from ref. [73] with permission from the Journal of Aerosol Science).

2.2.4 Working distance

The working distance between the substrate and nozzle directly affects the electric field force acting on the liquid droplets. If the working distance narrows down, the change in electric field force on the cone becomes faster when the same electric potential is applied, that is, the acceleration of a fluid jet toward a substrate would increase simultaneously. On the other hand, the meniscus surface charge aggregation rate would become slower, so at the same time, the electric field force will not be enough to break through liquid surface tension and internal viscous forces [78]. The unstable variation in injection frequency during production activities is caused by two main factors, which are (1) variation in standoff height due to liner tilt and (2) variations in local injection conditions for short periods (thickness and conductivity of the substrate are not uniform). Barton and coworkers used both SSCM and NSM to adjust the voltage difference between the tip and substrate according to the twodegree-of-freedom control law [79]. They found that variations in standoff height have been effectively compensated by adjusting injection frequencies. They also employed numerical simulations in their study to improve the stability of EHD on-demand printing.

2.2.5 Working speed

The working speed of an EHD printer is also known as the relative speed of its nozzle and the direction of its movement. In EHD printing, if the work speed is too fast, often due to a mismatch with the supply flow, it will result in the phenomenon of broken lines, and if the work speed is too slow, then it will result in too large printed pattern line width, and due to the deposition of more ink, evaporation is slow, the edge of the pattern accuracy is also reduced. As shown in Figure 8a and b, the line width increases with the increase in speed and the thickness decreases with the increase in speed in the working speed range of the line without breakage [80]. When the speed is too high, the line breaks as the radius of the jet becomes smaller with the increase in active driving force leading to the jet. At lower printing speeds, too much ink is deposited on the substrate, creating a bump and the surface flow of the printing ink creates a distended shape.

In conductive networks, thicker and wider lines provide higher conductivity but also lead to loss of light transmission. Therefore, controlling the aspect ratio (AR) of the wire by operating speed is an important means of regulating the device to achieve the desired performance, and obtaining a printed structure with a high AR [81].

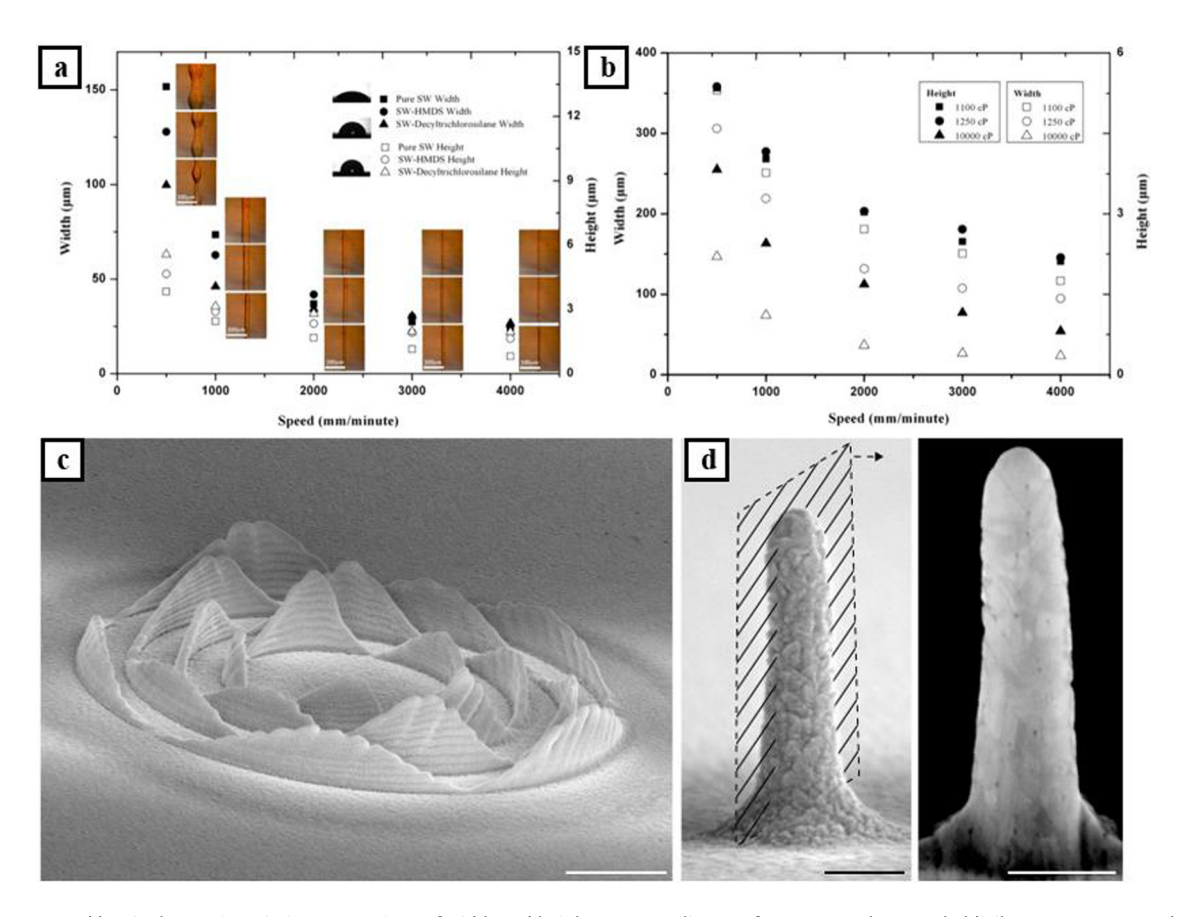


Figure 8: (a and b) Single EHD jet printing comparison of width and height on pure silicon wafer (SW), SW-hexamethyldisilazane treatment substrate, and SW-decyltrichlorosilane treatment substrate (reproduced from ref. [80] with permission from the Applied Physics Letters); (c and d) Geometric properties and post-print microstructure of printed stacks with high ARs (reproduced from ref. [82] with permission from Nature Communications).

Compared to the traditional printing, EHD printing achieves high print resolution by cone-jet or droplets much smaller than the actual nozzle size, and thus has a greater advantage in converting from 2D patterns to high precision and high AR 3D stacks. Using EHD redox printing, Reiser and coworkers achieved instant switching and mixing of two metals from a single multi-channel nozzle, printing patterns with a spatial resolution of up to 250 nm at an operating speed of 10 voxels per second and an AR of 400, as shown in Figure 8c and d [82].

2.3 Challenges in electrospinning and electrospray

Electrospinning and electrospray refer to EHD processes of the same technological origin. Both electrospray and electrospinning take advantage of the unstable EHD behavior [83]. The standard setup includes a syringe with the selected polymer solution, connection to the spinneret, syringe pump, grounded collector, and high voltage [84].

During electrospinning, the distance between the tip of the spinneret and the collector in terms of distance (H) determines at which stage the fibers will be deposited on the collector (as shown in Figure 9a) [85-87]. Conventional electrospinning is usually performed in far-field mode applying high voltages. For the fabrication of films or coatings with nanofiber structures (as shown in Figure 9b) [88–90], when the distance is reduced to 500 μ m to 5 cm, the electric field is highly concentrated between the spinneret and the collector, and near-field electrospinning is possible. In this way, the desired graphics can be printed with stable precision (as shown in Figure 9c) [91-93]. Polymer solutions with relatively low viscosity and high surface tension tend to electrospray into droplets or form fibers with beads embedded along their length (as shown in Figure 9d) [94,95].

2.3.1 Voltage control

The electrospinning mode of operation is formed by a combination of Coulombic, electric field, viscoelastic,

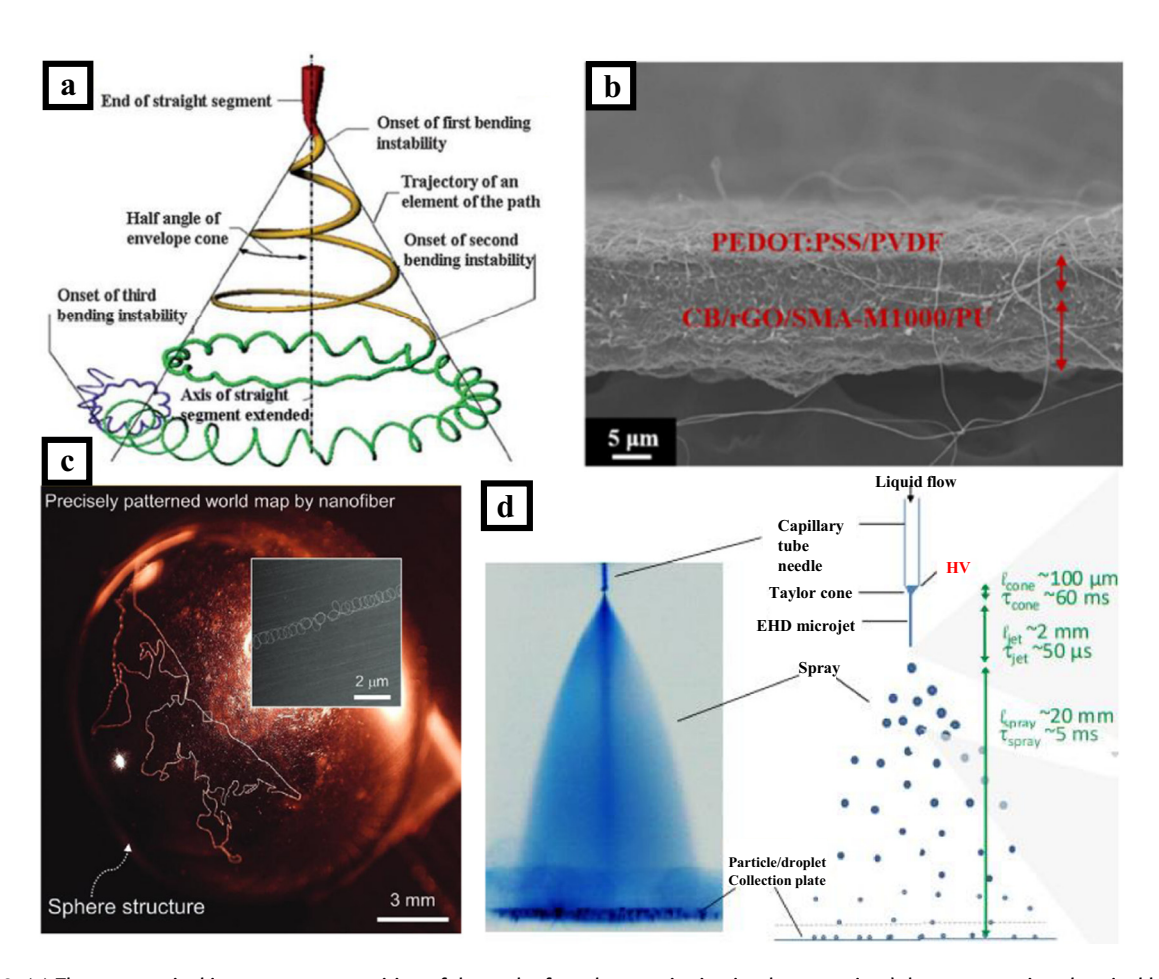


Figure 9: (a) The prototypical instantaneous position of the path of an electrospinning jet that contained three successive electrical bending instabilities (reproduced from ref. [87] with permission from Polymer). (b) Cross-sectional SEM image of the nanofiber carbon electrode (reproduced from ref. [90] with permission from ACS Applied Electronic Materials). (c) Precisely patterned world map by nanofiber on the sphere structure using self-aligning nanojet (reproduced from ref. [93] with permission from Advanced Materials Technologies). (d) Electrospray stages and length and time scales (reproduced from ref. [95] with permission from Journal of Aerosol Science).

and surface tension forces (Figure 9) [96], as shown in Figure 10. Larger applied voltages have greater electrostatic interactions in the charged solution, greater stretching occurs on the fluid jet, and greater repulsive forces are generated, resulting in the production of small diameter fibers [97]. Wang et al. tested the cone-jet diameter at different voltages (6.5-7.5 kV) for 17 wt% PNIPAM/DMF solution, and there was a reduction in the diameter by high voltage [98]. The external voltage also affects the morphology and arrangement of the fiber molecules. The average fiber diameter decreases as the applied voltage increases to a critical value due to the increased electrostatic force and tensile stress in the polymer solution [99]. Şener et al. investigated the effect of fiber forming in voltage changes and as the voltage increased from 28 to 35 kV, the fractured fibers improved. The nanofibers became continuous [100]. Jiyong et al. observed PVDF nanofibers at different applied voltages from 14 to 20 kV, and the nanofiber crystallinity

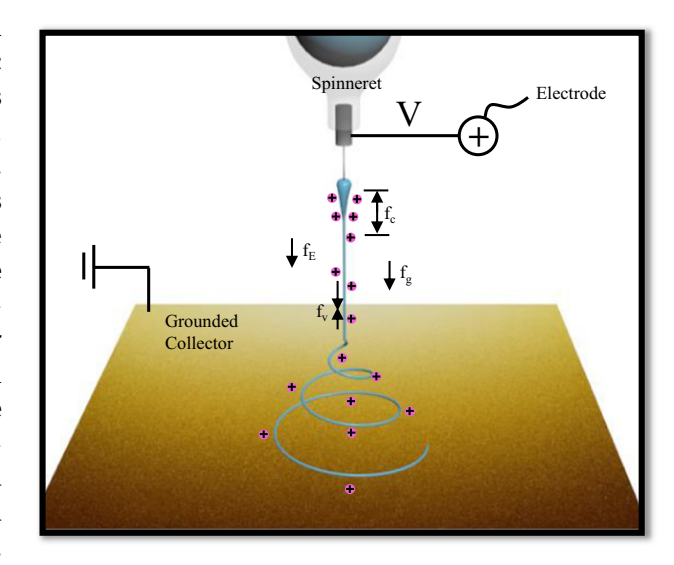


Figure 10: Schematic diagram of the action of different forces on the solution in the electrospinning mode of operation.

increased from 14 to 58%. The crystallinity supports most of the β -phase in the crystal structure. The results demonstrate a strong correlation between crystallinity and applied voltage [101].

2.3.2 Flow rate

Flow rate is considered one of the key parameters controlling fiber diameter and its distribution, initiating droplet shape, jet trajectory, Taylor cone maintenance, and deposition area [102–104]. As the flow rate increases, the size of the fibers and beads formed increases. In order to produce bead-free homogeneous fibers, a slower flow rate is usually used to provide sufficient polarization time for the polymer solution to allow sufficient time for the solvent to evaporate as well. At higher flow rates, the residual solvent may encourage the fibers to fuse together and form webs rather than fibers [105]. Zargham et al. observed the fiber morphology of nylon solution at different flow rates of (0.1–1.5 mL/h). By increasing the flow rate, the morphology of the fibers showed defects such as a larger droplet volume ratio and split fibers. The area density of the fibers decreased continuously as the solution flow rate increased [106]. Gee et al. compared the contribution of solvent ratio, tip to collector distance, flow rate, and voltage as influencing factors on β -phase formation. The flow rate was found to be second only to the solvent ratio for its formation; however, the relationship between the flow rate and the β -phase fraction was inconclusive. The highest average β-phase fraction was observed at 0.8 mL/h, which is quite different from the other two flow rate settings tested [107].

2.3.3 Speed matching model

In the near-field electrospinning mode, the relative velocity between the collector and the nozzle plays an important role in the deposition of fibers and is the most important influencing parameter in the accurate mapping process [93]. Curling or wavy deposition occurs when the jet impingement speed is relatively faster than the collector speed and is often applied in processes for coating or making polymer films. Fabrication of precision devices using near-field electrospinning is an emerging printing process, so it is critical to equalize the jet impingement speed to the collector speed for successful deposition of linear electrospinning fibers along complex curved paths [108-110]. Brown et al. combined predictable deposition positions of several types of melt electrostatic spun fibers with an

automated lateral translation collection system that can be drawn into continuous straight lines over a range of fiber diameters from the single micron-scale to 50 µm when the collector has optimal control while translating at a speed that matches the speed of the jet (Figure 11a and b) [111]. Bisht et al. found that the platform movement speed has a dramatic effect on the wire-forming diameter of nanofibers, with lower platform movement speeds leading to larger fibers and vice versa, most likely due to mechanical stretching of the nanofibers between the contact points on the substrate and the droplets (Figure 11c and d) [112].

Breakthroughs in EHD E-ink materials

EHD printing deposits ink on different types of substrates. Conductive ink is a basic material for a conductive pattern while developing printed electronics [113-117]. It is mainly composed of conductive filler, solvent, dispersant, binder, and various additives. As is pointed out, the accuracy of EHD printing is highly related to the electrical conductivity, fluidity, switching voltage, and critical voltage stability of the ink material [118]. According to the different conductive fillers, electronic ink can be divided into metal-system [119-123], carbon-system [124-128], and polymer-system conductive ink [129-132].

3.1 Metal conductive ink

Metallic materials have always been the first choice for conductive materials. Metal conductive inks can be divided into nanoparticle-based and particle-free conductive inks according to the presence of metals in a solution [133–135]. In order to achieve excellent electrical properties, many metal nanoparticles are used to prepare conductive printing inks for EHD printed electronic devices, such as gold nanoparticles, silver nanoparticles, and copper nanoparticles, to name a few. Nanoparticle conductive inks usually consist of metal nanoparticles or nanowires, volatile solvents and surfactants, and other additives. The main advantage of nanoparticle-based inks is the higher content of the metal conductive phase in ink.

Thi Thu Thuy Can and coworkers successfully deposited high-viscosity silver nanoparticles on indium tin oxide (ITO) glass using EHD jet printing method by adding effective additives such as propylene glycol methyl ether acetate (PGMEA) to the silver paste formulation. The results

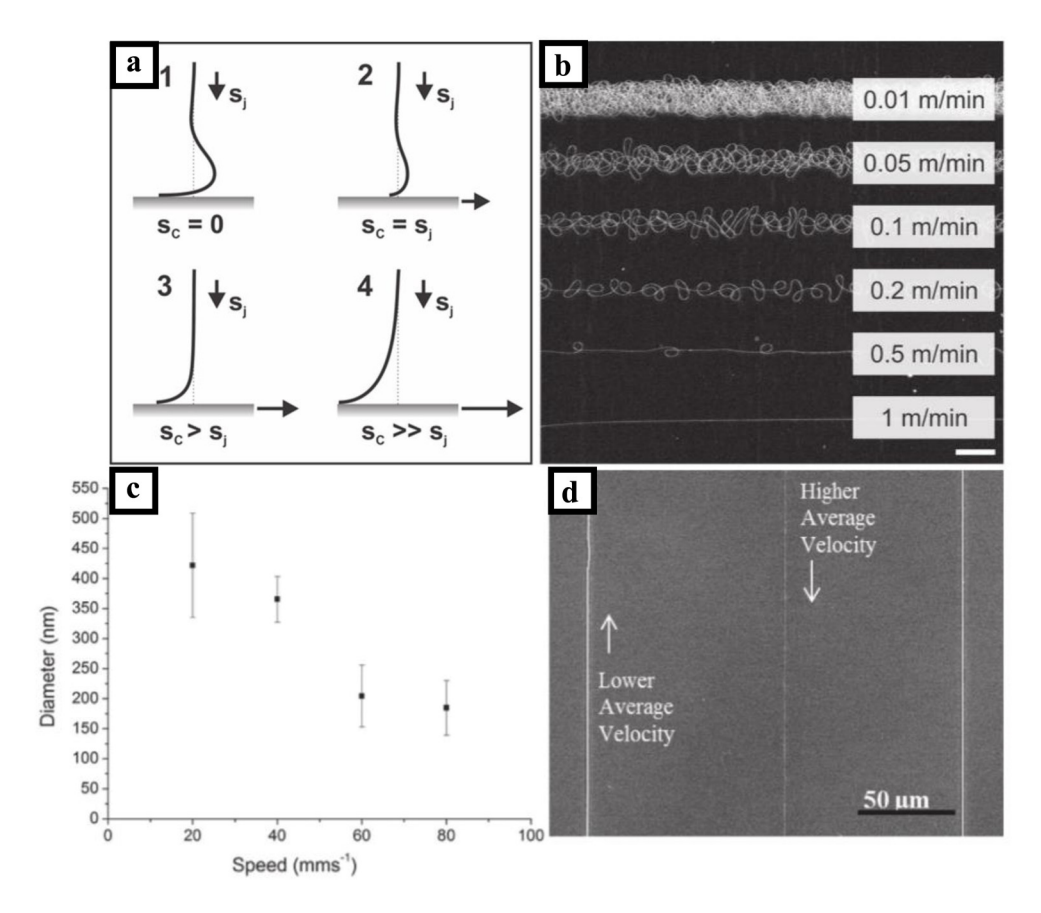


Figure 11: (a) Schematic showing that the shape of the melt electrospinning profile is dependent on the speed of the collector relative to the jet speed. (b) Photograph of lines of PCL fiber melts electrospinning at different collector horizontal speeds (reproduced from ref. [111] with permission from Advanced Materials). (c and d) Correlation between nanofibers thickness and stage speed (reproduced from ref. [112] with permission from Nano Letters).

showed that a linewidth of less than 100 µm was obtained, and the fabricated silver patterns were well organized with an average thin-layer resistance of about 0.027 Ω^{-1} . The fabricated thin-film transistors (TFTs) with zinc tin oxide (ZTO)/ SiO₂/Si have the mobility of 0.97 cm²/V s and a switching current ratio of more than 10⁶ (Figure 12a). It also demonstrated that the obtained patterns represented a new breakthrough for microelectronic fabrication [136]. In another work carried out by Han and Dong [137], they printed metallic wires directly using low melting point metallic inks - field's metal (32.5% bismuth, 51% indium, and 16.5% tin) with a resolution of less than 50 µm. As shown in Figure 12b–d, the EHD printed wires were tested with hundreds of bending and stretching/ releasing cycles under a wide range of tensile strains (0-70%). In addition, the printed metallic conductors exhibited selfhealing capability. Due to the in situ self-healing effect, faults in the circuit can be repaired by low-temperature heat treatment at 60°C without reducing its tensile properties.

Electrodes of silver nanowires (AgNWs) with high conductivity, transparency, and solution processability meet the needs of the flexible electronics industry for highly flexible and transparent electrodes [138-142]. Li used EHD printing to fabricate IG-coated AgNW electrodes with high flexibility and mechanical resistance on a flexible polyethylene terephthalate (PET) substrate [143]. There was no change in the electrical resistance while the IG-coated AgNWs electrode was fully immersed in the water and isopropyl alcohol solution because the IG coating protected the AgNWs electrode keeping it from electrochemical permeation (Figure 12e). Jin used the $(Ba_{0.85}Ca_{0.15})(Ti_{0.9}Zr_{0.1})O_3$ (BCTZ)NWs and Cu@Ag particles to fabricate E-ink for EHD printing [144]. This is because the Ag coating of Cu@Ag particles can protect the copper core from being oxidized and can improve the oxidation stability of Cu@Ag particles. The oxidative stability of Cu-Ag was verified to be superior to that of Cu nanoparticles according to Lee et al. [145]. The resistivity of Cu-Ag core-shell conductive ink was measured as 12.0 $\mu\Omega$ /cm at 350°C. The results indicated that the Cu-Ag core-shell nanoparticles have better electrical

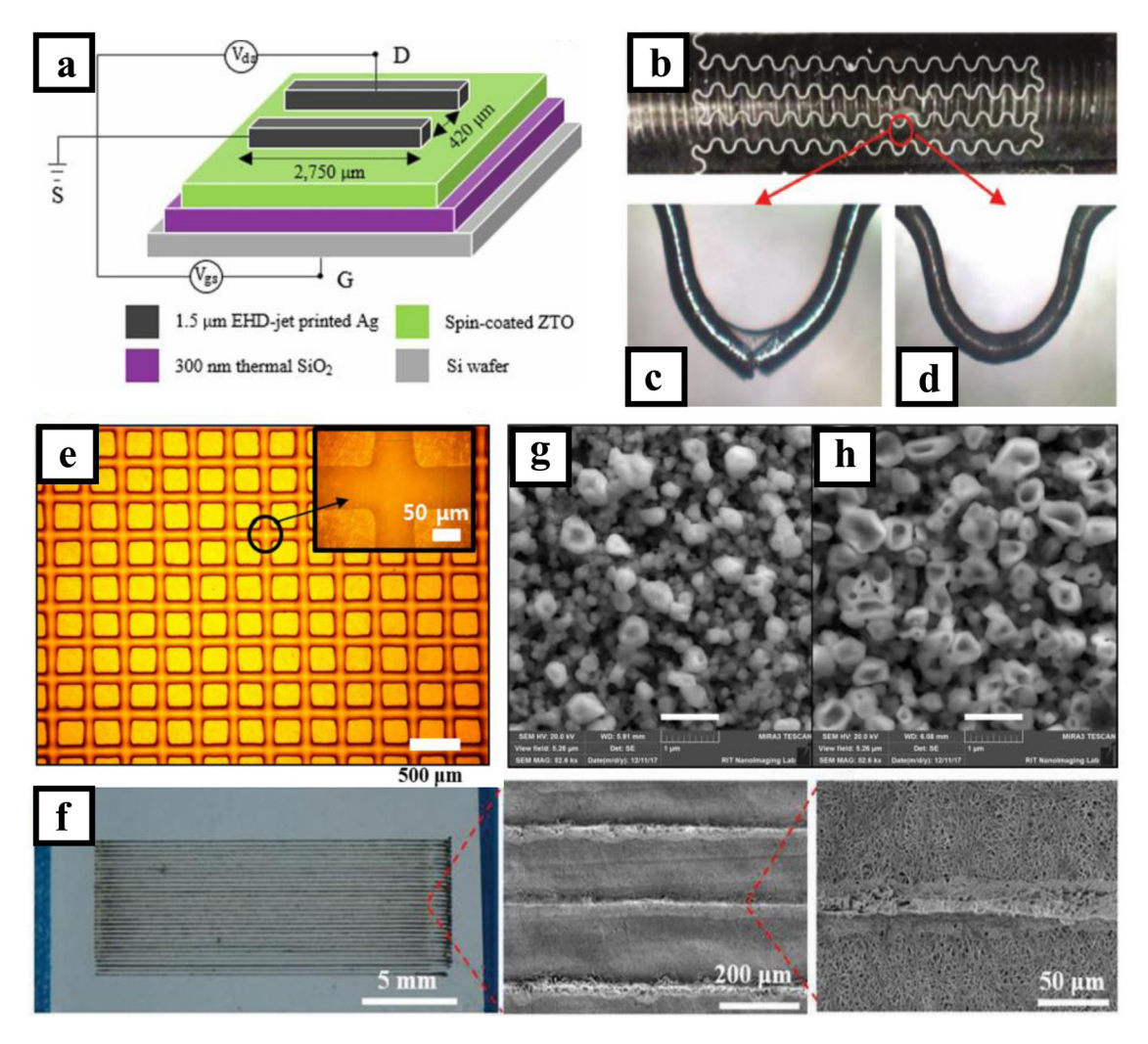


Figure 12: (a) Schematic representative of the cross-sectional view of a ZTO TFT with printed Ag S/D (reproduced from ref. [136] with permission from Nature). (b) A chain of connected half-circle patterns under multiple stretching-failure-healing tests. (c) Optical images of a failure location before and (d) after healing (Figure 9b–d reproduced from ref. [137] with permission from the Advanced Materials Technology). (e) Optical images of EHD printed grid patterns where AgNWs are coated with transparent IG solution (reproduced from ref. [143] with permission from Organic Electronics). (f) Photograph and SEM images of Ag-PEO features on an electrospun nanofibrous poly(L-lactic acid) film (reproduced from ref. [153] with permission from Journal of Materials Chemistry C). (g) Thermal curing at 120°C for 5 min. (h) Photonic curing (3.3]/cm² for 250 μs) (reproduced from ref. [154] with permission from ACS Applied Materials & Interfaces).

properties than Cu nanoparticles. Compared with Ag particles, Cu@Ag particles have a lower cost and are considered to be potential low-cost fillers in the future.

However, there is always a challenge when applying nanoparticle conductive inks for EHD printing electronics, such as the clogging of nozzles. Particleless conductive inks are definitely one of the most promising solutions for the clogging of nozzles, for example, inks with metal components in ionic form. Within this system, metal precursors play a decisive role in the conductivity of a pattern after heat treatment. Usually, silver precursors were used, including silver citrate [146], silver neodecanoate [147], silver oxalate [148], silver carbonate [149], silver acetate

[150], silver nitrate [151], and silver tartarate [152], to name a few. Lei and coworkers developed an EHD printing method using silver acetate as a precursor [153]. Based on *in situ* reactive inks, they prepared micron-scale conductive silver patterns with tunable resistance on various flexible substrates at a mild temperature (90°C), obtaining a minimum linewidth of 27.6 \pm 3.4 μ m and a conductivity of 3.3 \times 10⁶ (Figure 12f). In the work by Zope *et al.* [154], they first formulated silver ink with 29.5% silver content using silver oxalate as a precursor and then inkjet printed the ink on various substrates. The ink performed well when heated at 120°C for less than 5 min, but when photonic curing was introduced, substantial improvements were made.

Enhanced conductivity in the photonically cured silver films was reflected in the morphology observed in the SEM images (Figure 12g and h). After a hybrid thermal and photonic sintering curing, silver films with a resistivity of $4.26 \times 10^{-8} \, \Omega/m$ were developed, which exhibited great potential in electronics.

3.2 Carbon based ink

Carbon materials are used more often as conductive fillers due to their good conductivity and ease of building conductive pathways. The main carbon-based materials used as conductive fillers are carbon nanotubes (CNT), graphene, and conductive carbon black (CB). There is another type of carbon structure, which consists of a number of columnar carbon tubes coaxially nested, with diameters ranging from 1 to 30 nm and lengths up to 1 μ m [155].

Advantages of CNT-based inks over metal-based inks include higher oxidation resistance and electromigration resistance. Composites of CNT and copper nanoparticles have shown excellent conductivity (Figure 13) [156]. However,

due to the strong van der Waals force, CNTs are not easy to disperse in solvents. Jeong and coworkers developed a multi-walled CNT (MWCNT)/polystyrene composite ink for EHD patterned conductive wires [157]. In their study, the multi-walled CNT/polystyrene wires were used as sulfur/sulfur electrodes for organic field-effect transistors (OFETs) deposited on polystyrene brush modified surfaces. These devices showed excellent/reliable electrical performance and no electrical system failure.

Graphene plasmons are rapidly emerging as a viable tool for fast electrical manipulation of light. The prospects for applications in electro-optical modulation, optical sensing, quantum plasmonics, light-harvesting, spectral photometry, and tunable lighting at the nanoscale are further stimulated by the relatively low level of losses and a high degree of spatial confinement that characterize these excitations compared with conventional plasmonic materials, alongside the large nonlinear response of graphene [158–160]. Ali and coworkers used EHD printing to fabricate a stretchable photosensor, a photoconductive layer of perylene/graphene (66 nm), and ITO electrodes on a uniform ridged Polydimethylsiloxane (PDMS) substrate [161]. The maximum detectable light intensity by

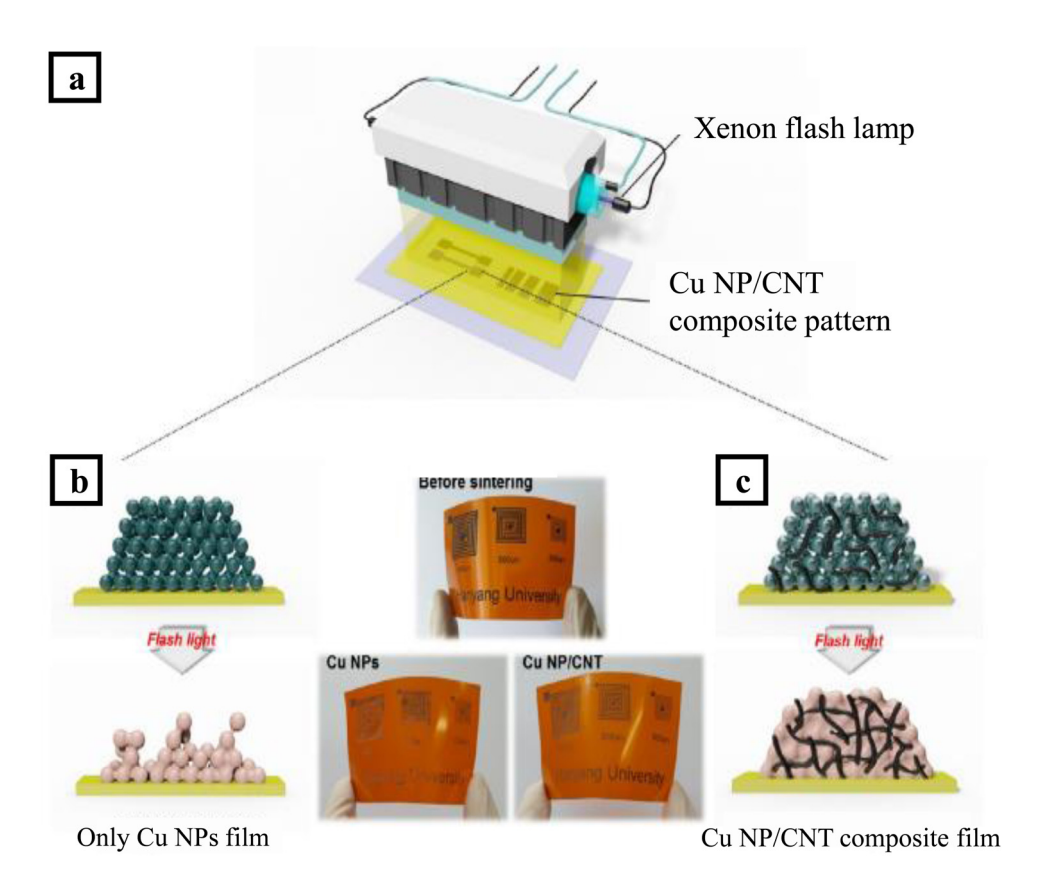


Figure 13: (a) Schematics of the flashlight sintering system and (b) the shape change comparison of CuNPs film only, and (c) CuNP/CNT composite film after flashlight irradiation (reproduced from ref. [156] with permission from ACS Applied Materials & Interfaces).

the sensor was 400 lux and its detectable range was from 465 to 535 nm in a visible spectrum.

Conductive CB has small particle size, high structure, pure surface, rough and hollow, and other characteristics, which enable products conductive to own low resistance and high conductivity. It can effectively form a 3D mesh structure in an insulator, which in turn effectively improves its electrical conductivity. Hwang and coworkers developed a CB/TX-100 composite ink for EHD patterned wires [162]. The CB/TX-100 was used as an S/D electrode for TIPS-para phenylene OFETs. The results showed that the OFETs with CB/TX-100 S/D electrodes exhibited better electrical performance in terms of transfer/output characteristics and smaller hysteresis (average carrier mobility of 0.165 cm²/V s and on/off ratio of about 10⁵) compared to TIPS-pentacene OFETs and gold S/D electrodes (bottom contact), which was attributed to the CB/TX-100 electrode and better crystal matching of the crystals on the silica channel region with edge orientation. Their study demonstrated a bright future for EHD printing of carbon-based composites and their applications in next-generation electronic devices.

3.3 Polymer ink

Polymeric conductive inks are of great value in both scientific research and industrial applications. Currently, the most commonly used conductive polymers are poly(3,4ethylenedioxythiophene):polystyrene sulfonate (PEDOT: PSS). It has characteristics including high electrical conductivity and excellent environmental stability. Chang and coworkers successfully prepared micro-PEDOT: PSS-PEO with tunable conductive and thermal properties for flexible polymer substrates [163]. By using an insulating substrate and a working distance of 100 µm, the discharge problem in the conical injection mode was successfully solved. The minimum width printed on PLGA substrates was about $27.25 \pm 3.76 \,\mu\text{m}$. By controlling the number of stacked layers, the resistance of multilayer features can be tuned from 16.02 \pm 1.70 to 0.77 \pm 0.05 k ω /cm. And the thermal properties could be flexibly adjusted. The team achieved the fabrication of miniature PEDOT: PSS-PEO electronic devices with tunable conductive and thermal characteristics directly on flexible polymer substrates at low temperatures (<50°C) in conical injection mode (Figure 14a).

PDMS is one kind of polymer organic silicide, consisting of a chain structure with different degrees of polymerization. PDMS is widely used as biomaterials in many fields, such as biology, medical science, and microfluidics, because of its good biocompatibility, optical transparency,

high structural flexibility, and low cost [164]. The printing process of PDMS ink was investigated by Jiang et al. By designing the pulse voltage and pulse frequency, the PDMS droplet size and printing frequency had been precisely controlled. It pointed out that an increase in the pulse voltage and frequency led to an increase in printing frequency and a reduction in PDMS droplet size. The relationship between printing frequency and pulse frequency is close to linear, indicating that the printing frequency can be precisely controlled by the pulse frequency (Figure 14b).

In another work by Vijavavenkataraman et al. [165], polycaprolactone (PCL)/polyacrylic acid (PAA) nanocomposites were used as polymeric ink for EHD printing. The conductivity range of the PCL/PAA scaffold matched that of the myelin sheath of amphibian motor nerve fibers, approximately 10^{-6} S/cm. The mechanical properties of the scaffold decreased as the concentration of PAA increased, and the degradation rate was accelerated. Thus, by varying the concentration ratio of PCL to PAA, the mechanical properties and biodegradability could be adjusted according to the injury and site-specific requirements. In vitro cellular studies with PC12 cells, it demonstrated that PCL/PAA scaffolds supported cell proliferation, growth, and neural differentiation better than pure PCL scaffolds. As is pointed out, EHD-injected 3D-printed porous conductive PCL/PAA neuroglia has the potential to be used for the treatment of peripheral nerve injury and may be extended to other neural tissues (Figure 14c and d).

4 Demanding devices from EHD printing

EHD printing has become a current research hot printing technology for fabricating devices such as transistors, sensors, electroluminescent devices, and super miniature capacitors due to its wide adaptability to solution materials, high accuracy of device printing, and its versatility in fabricating different microstructured surfaces with multiple modes of operation. Many researchers have written reviews for specific research areas, and we have summarized their reviews as shown in Table 2. We also summarize the last 5 years of research in different fields of EHD printing of high-performance devices.

4.1 TFT devices

TFTs are insulated gate type field-effect transistors that use a gate voltage to generate a vertically oriented electric 3320 — Chenhao Cong et al. DE GRUYTER

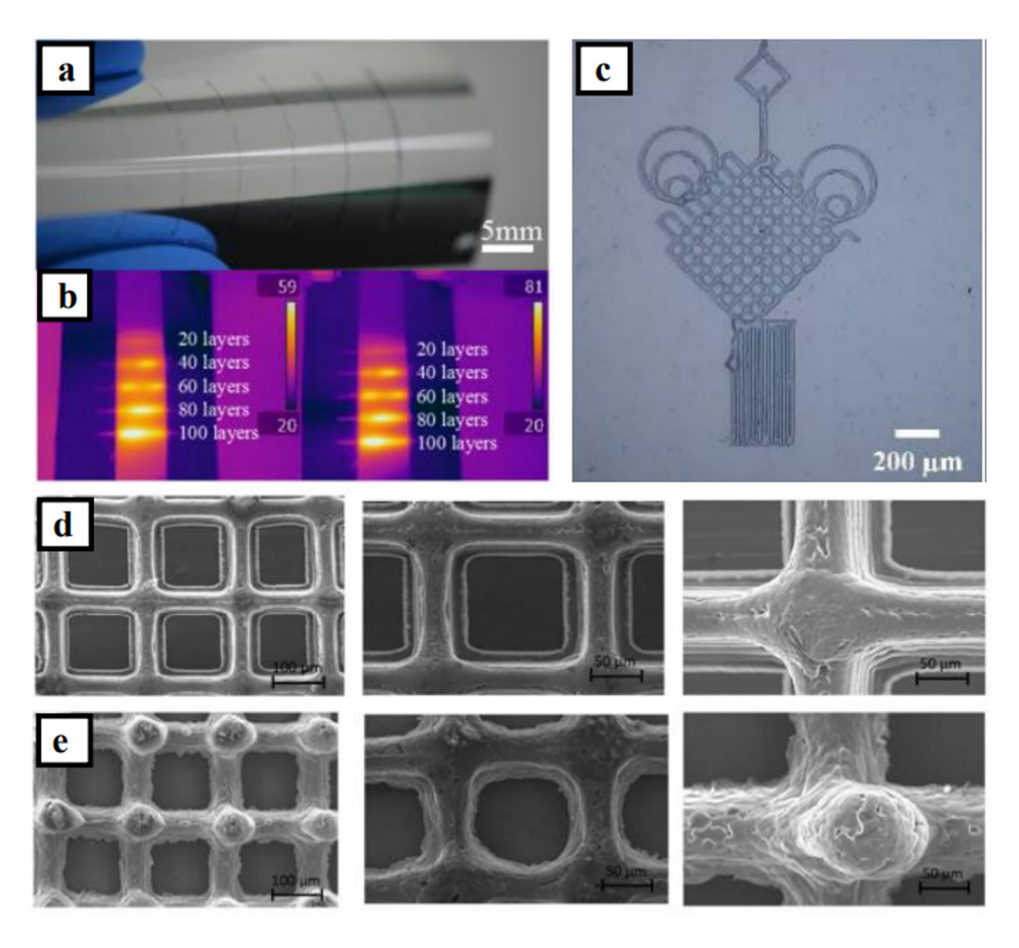


Figure 14: (a) EHD printing of microscale conductive lines with gradient layer number on a flexible PET film. (b) Infrared thermal images to show gradient distribution of maximum temperature of the printed features (reproduced from ref. [163] with permission from ACS applied materials & interfaces). (c) Printed patterns: Chinese knot (reproduced from ref. [166] with permission from Procedia Manufacturing). (d) SEM images of scaffolds fabricated for NGCs using 3D printing assisted EHD jetting PCL scaffolds. (e) PCL/PAA 7.5% at different magnifications (reproduced from ref. [165] with permission from Materials & Design).

field thus controlling a carrier change. Oxide TFT has higher field-effect mobility than amorphous silicon TFT, but has lower process cost than polysilicon TFT. The focus of current related research on oxide TFTs includes ZTO, indium oxide (In₂O₃), indium gallium zinc oxide (IGZO), etc. [171–173]. Most oxide TFTs are fabricated using vacuum techniques such as atomic layer deposition, DC or RF sputtering, and ion beam deposition [174-176]. The disadvantages of the vacuum process are that it is not suitable for large area deposition and is expensive. Instead, solution methods are proposed because they are simpler and more environmentally friendly than vacuum methods. Representative solution methods include spin coating, inkjet printing, screen printing, gravure printing, and EHD printing. Especially EHD printing can produce patterns of any ink formulation with an electrical charge while with less dependence on viscosity.

Can and coworkers synthesized MoS_2 precursors by a solution method and obtained linear MoS_2 patterns using

an EHD printer [177]. Compared to spin-coated films, the morphology of MoS₂ after a transfer process remained free of folds or cracks. The EHD jet-printed MoS₂ was then transferred on a high-k Al₂O₃ dielectric, forming a semiconductor layer in TFT applications. The printed MoS₂ TFTs had electrical properties including linear field-effect mobility 47.64 \pm 2.99 cm²/V s, current ratio 7.39 \pm 0.12 \times 10⁶, and low subthreshold swing 0.7 \pm 0.05 V/decade.

Liang and coworkers developed all-metal oxide TFTs by EHD printing semiconductor metal oxide (In₂O₃ or IGZO), dielectric layer (Al₂O₃), and tin-doped ITO for source-drain and gate [178]. The feature size of the high-performance transparent electronic device was less than 2 μm . The EHD printed TFT had electrical properties including average saturation mobility of 117.2 \pm 38 cm²/V s and an average threshold of $-0.41\,V$. In another study by Yong et~al. [179], they fabricated fully solution-treated transparent synaptic transistors for production capable of mimicking biological

Table 2: Summary of recent reviews on EHD printing in applications

Reference	Objective	Database/ publication year	Search terms	Conclusions
Xu et al., 2019 [129]	EHD printing allows control of the nanowire gap and diameter to optimize the electrical properties of transistor-based devices	Database: Springer Year: published on September 16, 2019	<i>Terms</i> : nanowire array; oxide nanowires; transistor	The molecular structure of the source material and its nanoscale aggregation behavior in the nanowires can significantly affect the electrical or optical properties of the printed nanowires. Second, the diameter of nanowires can be controlled by solution concentration and viscosity, which is easier to achieve than
Shao and Wan, 2019 [167]	The low viscosity ink of the inorganic precursors makes the EHD jet printing-based method a better choice for printing inorganic materials, with significant advantages in printing oxide transistors in a way that offers high print resolution and adaptability to high viscosity inks	Database: IOPscience Year: Published on February 1, 2019	<i>Terms</i> : TFTs; oxide-based semiconductors; jet printing;	At the device level, jet-printed metal oxide TFTs show fundamental properties comparable to those of vacuum-prepared TFTs. At the same time, the availability of ion-based dielectrics has promoted the application of in-plane gate structures, which are particularly suitable for depositing ion-based dielectrics by jet printing, and the availability of water-based graphene motor ink, whose good contact quality with metal oxides contributes to the performance of metal oxide transistors
Chen <i>et al.</i> , 2019 [168]	The materials prepared by electrostatic spinning technology have ultra-long length, large specific surface area, and high porosity, which greatly improve the sensitivity and response time of electrochemical sensors	Database: Multidisciplinary Digital Publishing Institute Year: Published on August 23, 2019	<i>Terms:</i> electrochemical sensors; glucose; hydrogen peroxide; nanomaterials	Electrospinning nanofibers have ultra-long length, large specific surface area, high porosity, and excellent mechanical properties. In addition, by combining electrostatic spinning with other techniques, nanomaterials can be dispersed as additives in nanofibers or nanofiber membranes to fabricate enzyme sensors and non-enzymatic sensors. In non-enzymatic sensors, the surface structure of electrostatically spun nanofibers can yield new, specialized electrodes to fabricate fiber structures with controlled size, structure, and high chemical activity
He <i>et al.</i> , 2020 [169]	Recent advances in high-resolution EHD bioprinting technologies are reviewed, mainly including melt and solution methods for the preparation of micro/nanofibrous scaffolds and living tissue structures	Database: The American Society of Mechanical Engineers Year: published on November 29, 2018	<i>Terms</i> : bioprinting; tissue engineering; biofabrication	The fiber size of EHD bioprinting based on molten biopolymers is close to cell size, providing an ideal way to simulate the microfibrous structure of natural extracellular matrix. Biopolymer solutions have higher resolution in EHD printing down to sub-micro-scale or even nano-scale. For cellular tissue structures, EHD bioprinting still falls short in providing the necessary growth microenvironment for the proliferation of

Table 2: Continued

Reference	Objective	Database/ publication year	Search terms	Conclusions
				encapsulated cells and the printing accuracy needs to be improved to obtain better cellular tissues
2022 [170]	of uniform thin films at the micro/nanoscale for the manufacture of solar cells, photodetectors, light emitting diodes (LEDs), and transparent electrodes using more complex high specific surface area patterns, demonstrating that EHD printing shows significant advantages in multimode tunability and its application in the deposition of various optoelectronic materials and device preparation	Database: Royal Society of Chemistry Year: First published on August 10, 2022	FHD deposition	erb jets can be used for electrospray generation of droplets, electrostatic spinning to generate micro/nano fibers, and EHD jet printing to generate micro/nano droplets, making it suitable for the fabrication of optoelectronic devices as it can meet all requirements for high performance solar cells (uniform thin films), displays (high resolution graphics), and sensors/detectors (large specific surface area structures). However, EHD deposition technology is just beginning to be investigated in optoelectronics, and device
				efficiencies in solar cells and LEDs lag far behind traditional processes such as spin coating or
				vacuum evaporation (<18% vs >29% device
				efficiency for solar cells and <5% vs >25% device
				efficiency for light emitting devices)

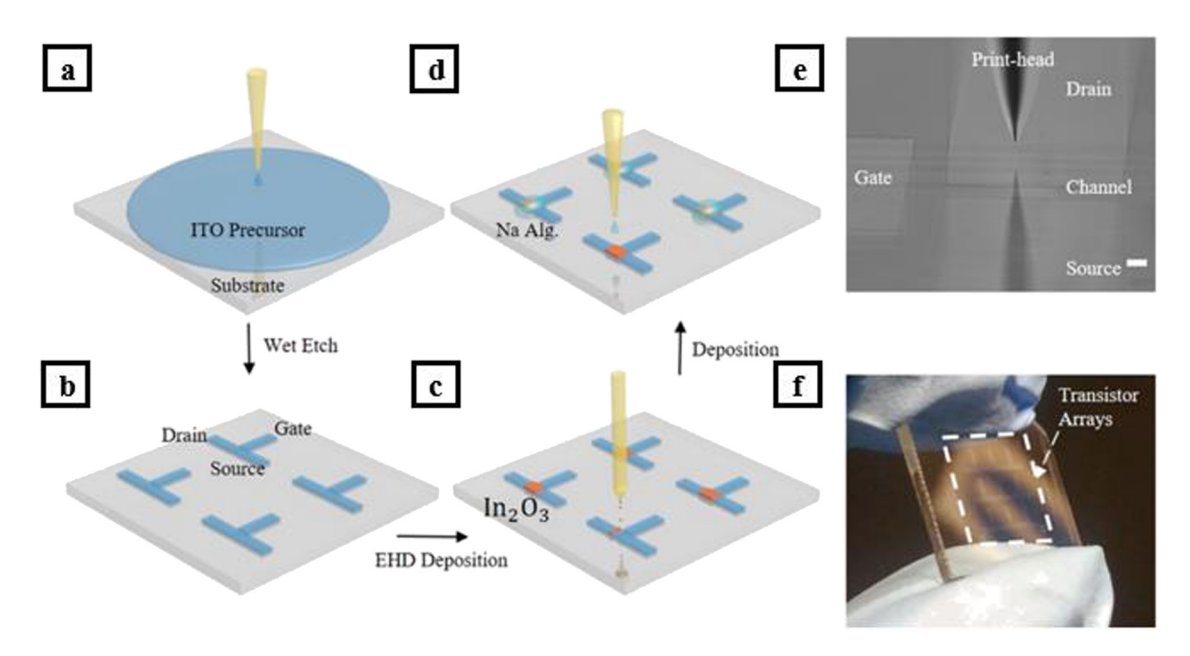


Figure 15: (a)—(f) Schematic representation of the fully solution-processed synaptic network using metal salt combustion precursors and the transistor morphology (reproduced from ref. [179] with permission from ACS Applied Materials & Interfaces).

synaptic functions and thus for building artificial neural networks. It was demonstrated that the sodium alginate-gated $\rm In_2O_3$ -gated transistor can form a basic building block for implementing artificial neural networks. The proposed transistor was intrinsically capable of short-term synaptic plasticity, as shown in Figure 15a–f. It can be used to mimic synaptic functions, which will allow the development of more complex neural networks with more sophisticated neural computations in the future.

4.2 Flexible sensors

Flexible sensors are widely used in many smart inspection devices. Their applications have been penetrated into various aspects of industrial production, marine exploration, environmental protection, and medical diagnosis [180]. As part of a one-step molding or manufacturing process, EHD printing plays an important role in this area. Typically, flexible sensors include flexible humidity sensors [181], flexible temperature sensors [182], flexible gas sensors [183], flexible pressure sensors [184], flexible strain sensors [185], and flexible thermal flow sensors [186], to name a few.

4.2.1 Flexible sensors of humidity and temperature

Low-cost temperature and humidity sensors have potential applications in agriculture, food monitoring, and

medical and industrial environments. How to make the temperature and humidity not affect each other is the current challenge to overcome [187]. Yousaf and coworkers presented a demonstration of a temperature-compensated integrated sensor set, of which sensor electrodes were fabricated using EHD on-demand printing technique, while the active films of the humidity sensors were deposited using the electrospray deposition method [188]. Curved silver patterns were used as resistive temperature sensors and cross-finger sensor (IDT) electrodes were used for humidity sensors. The total size of the final integrated sensor pair was 1.8 mm by 0.8 mm. The integrated sensor was capable of measuring temperatures in the range of 0-100°C with a sensitivity of 0.7Ω /°C and an average error of 1.5%. The second part of the integrated sensor was capable of measuring 0-80% relative humidity (RH) with a sensitivity of $85 \text{ k}\Omega/\%$ RH. The response and recovery time was able to be contained within 0.6 and 0.3 s, respectively. Besides the experimental study, a mathematical model was developed for real-time compensation of the RH sensor's resistive output response to temperature changes. The experiment proved to be a great leap forward for all printed high-sensitivity temperature compensated inexpensive commercial RH sensors with the developed solution.

Ali and coworkers deposited a composite methyl red/ graphene film layer on a silver electrode by EHD printing with a thickness of approximately 300 nm. Results confirmed that the resistance of the sensor decreased from 11 to $0.4\,\mathrm{m}\Omega$ relative to humidity of 5–95% [189]. Fabrication of the high-sensitivity sensor was successfully accomplished due to a combination between the methyl red/graphene composite film and the electrodes (Figure 16a).

4.2.2 Flexible gas sensors

Gas sensors are crucial for the detection of harmful gases in a variety of settings, including mining operations, industrial factories, livestock farms, *etc*. Most of the gas sensors are based on the use of semiconductor metal oxide nanostructures at room temperature. However, flexibility and/or stretchability is a challenge faced by advanced gas sensors [190]. Kang and coworkers investigated and developed an electrospinning metal oxide nanofiber micropatterning method based on EHD printing process [191]. Several types of metal oxide (tin dioxide, indium oxide, WO₃, and In₂O₃) nanofibers were produced by electrospinning, broken into smaller pieces by ultrasonic waves, and dissolved in organic solvents to be used as printing inks. Micro-scale electrospinning nanofiber patterns with a

minimum diameter of less than $50 \, \mu m$ were successfully achieved (Figure 16b). Advanced gas sensors were fabricated by EHD printing on microelectrodes and then used to detect toxic gases such as NO_2 , CO, and H_2S . The four metal oxides can detect NO_2 down to 0.1 ppm, CO at $20 \, ppm$, and H_2S at 1 ppm.

4.2.3 Flexible pressure sensors

Pressure sensors have been in commercial use in a variety of applications for over 30 years, such as touchpads, tactile devices, and fluid detection, to name a few. Touch activity is recognized by detecting small changes in the electrical charge generated by contact with fingers. These sensors usually consist of narrow wires. Because of this, they exhibit excellent sensitivity and are unaffected by most contaminants.

Qin and coworkers fabricated capacitive touch sensors based on E-jet printing using silver nano-inks on PET flexible substrates [192]. They proposed an improved mathematical model for coplanar contact sensor design,

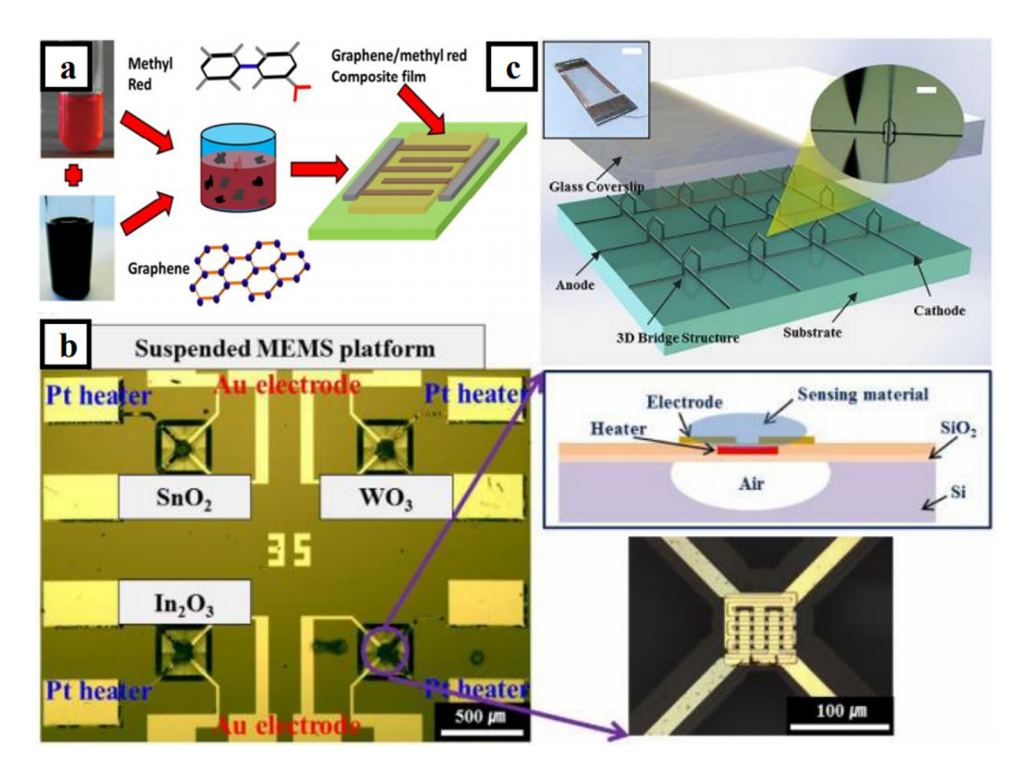


Figure 16: (a) Schematic representation of the graphene/methyl red composite-based humidity sensor (reproduced from ref. [189] with permission from Carbon). (b) MEMS gas sensor array fabricated by EHD printing of SnO_2 , WO_3 , and In_2O_3 nanofibers for low power consumption. The platform size is 3.5 mm \times 3.5 mm (reproduced from ref. [191] with permission from Sensors and Actuators B: Chemical). (c) 3D touch sensors were fabricated using the self-sintering EHD inkjet nanoscale 3D-printing technique. Schematic illustration of a 3D touch sensor and a magnified photograph of the 3D bridge-like structure as the capacitance unit (reproduced from ref. [193] with permission from ACS Applied Materials & Interfaces).

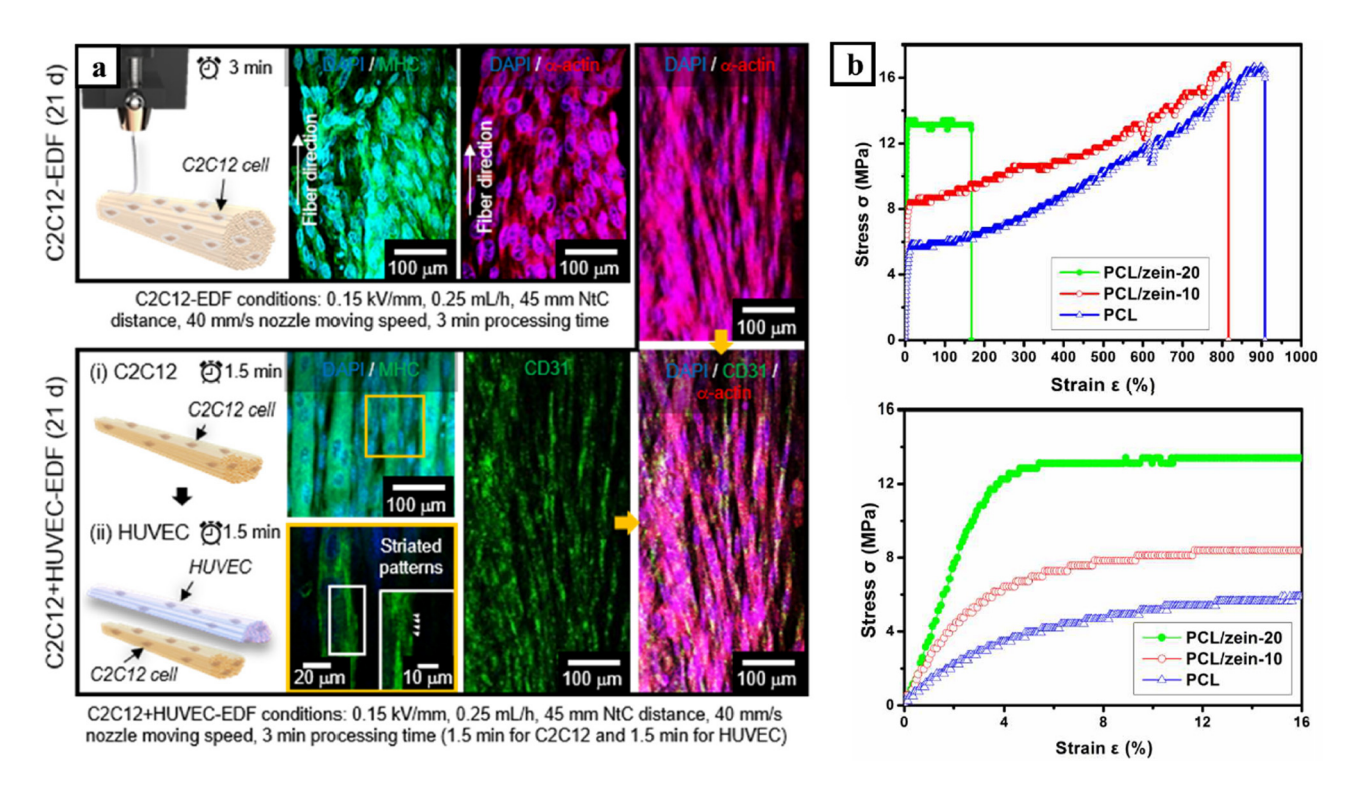


Figure 17: (a) Schematic and DAPI/MHC/sarcomeric α-actin/CD31 staining images of C2C12-laden EHD-DW fibers (C2C12-EDF) and C2C12/ HUVEC-laden EHD-DW fibers (CH-EDF) (reproduced from ref. [201] with permission from Carbohydrate Polymers). (b) Stress-strain curve of PCL, PCL/zein-10, and PCL/zein-20 scaffolds (reproduced from ref. [204] with permission from ACS Appl. Mater. Interfaces).

which successfully helped the fabrication of touch sensors with sub-20 µm electrode arrays using comb crossed digital structures. They found that the sintering conditions of ink droplets greatly affect the printing resolution, conductivity, and mechanical strength of 3D structures. In another study by Zhang et al. [193], they proposed a submicron EHD-based inkjet 3D printing technique that does not require an additional post-sintering process. The self-sintering phenomenon is particularly evident on conductive substrates and the proposed bridge-like 3D structure, which is constructed at a sub-10 µm scale level (Figure 16c).

4.2.4 Flexible bio-sensors

Flexible sensors are a hot topic in the field of biomedicine. The emergence of implantable and wearable medical devices has made the use of biomedical sensors less limited to specific areas and more beneficial for long-term real-time monitoring of patients' health conditions [194–196]. Go and coworkers synthesized one-dimensional silver column array electrodes modified with CNT and Pt nanoparticles using EHD inkjet printing technology [197]. The glucose sensor was made by infiltrating glucose oxidase as a detection part of the glucose detector into a silver column pre-coated with a mixture of MWCNT, Nafion, and platinum nanoparticles. The glucose detection range of Ag/ CNT + Pt_{nano} was between 5 and 555 µM and the Ag/CNT + Pt_{nano} glucose electrode was between 5.6 and 166.5 µM, with a sensitivity of $0.075 \,\mu\text{A}/\mu\text{M}$ and a low detection limit of 5.6 µM. And they tested the self-sintering phenomenon of AgNPs at 300 µm. The results showed that the aggregates were almost molten and sintered.

4.3 Biomedical field

In addition to biosensor applications, the use of EHD printing for the fabrication of pro-biotic base structures is also gaining attention. Due to the soft tissue of human organs, EHD-printed flexible electronics need to be compatible with various applications in the healthcare industry. In addition to their properties, such as their printability and compatibility with the human body, other factors, such as their stretchability, are also taken into account to ensure that these materials can be used in the medical field. Some electronic devices have already been implanted in humans [198-200].

Due to the complexity of the biomedical field, the need for high-resolution patterning is often required for various applications. One of the most common factors that can affect the cell activity is the presence of environmental conditions. EHD printing can avoid the use of photoresist and has a lower impact on the cell activity at low voltages. In order to achieve the desired cell activity and growth, Yeo and Kim used the EHD-printing direct-write (EHD-DW) mode to apply fibronectin to the bioink [201]. Through this method, he was able to successfully create microfibrous structures that are aligned with the microscale fibers. In addition to this, the direct writing mode also allowed the production of live cells that are loaded with fibronectin. The results of the experiment showed that the EHD printed flexible electronics were able to induce the growth of myogenic cells. The results of the tests revealed that the C2C12 myogenic and endothelial cells exhibited normal cellular activity (Figure 17a). These results indicated that the EHD-DW mode could potentially be used to produce tissue that is designed to treat human muscle loss.

EHD printing can also be used to create bio-scaffolds that are characterized by their mechanical properties. They can support the production of various protein and cellular structures *in vitro* and *in vivo* [202]. He and coworkers successfully prepared PEO-PCL-MWCNT composite microfiber scaffolds using solvent-based EHD printing [203]. The diameter of the printed fibers was about 10 μ m, which is close to the size of a living cell. Significant cell proliferation of

H9C2 rat cardiomyocytes was found on the PEO-PCL-MWCNT scaffold. In addition, MWCNTs were found to contribute to cell elongation and alignment with microfibrils. Properly functionalized CNT exhibited better biocompatibility and was even biodegradable, showing great potential for applications in biomedical and nanomedical fields.

The mechanical properties of bio-scaffolds are mainly influenced by the complexity of the biological tissues and organs they are designed to address. Since the devices' surfaces are constantly changing, the mechanical strength of the materials used for the production of these structures is the basis for their design. Jing $et\ al.$ developed a series of PCL/Zein composite ink-printed scaffolds with significantly better mechanical strength in terms of Young's modulus and yield stress, with strain limits of 802.8 \pm 59.1% for PCL/zein-10 and Young's modulus larger than 241.4 \pm 7.9 MPa [204]. Figure 17b shows the stress–strain curves of PCL, PCL/Zein-10, and PCL/Zein-20, and the biological scaffolds printed with EHD have potential applications in drug delivery systems, 3D cell culture models, and tissue engineering.

4.4 Electroluminescent devices

Due to the high resolution of EHD printing, it has unique advantages for printed electroluminescent devices. It has been well-known that the smaller the microlens, the more

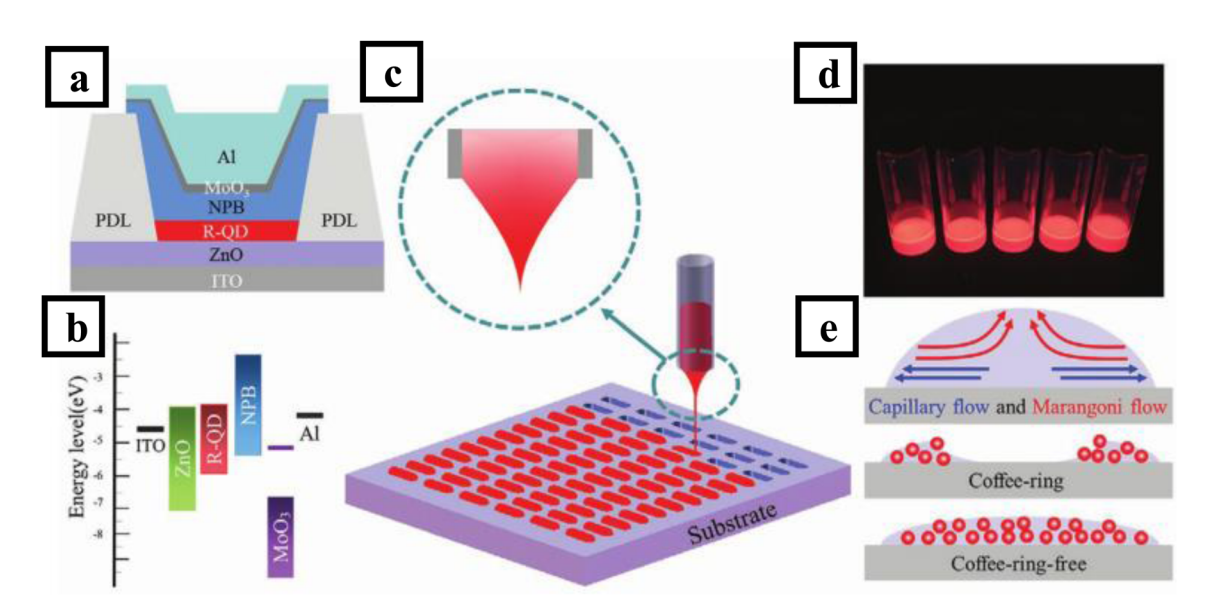


Figure 18: (a) Structure diagram of the QLED device. (b) Energy level diagram of the QLED. (c) Schematic of EHD printing to fill the pixel. (d) Image of QD inks with different solvent volume ratios, CHB: nonane is 10:0, 9:1, 8:2, 7:3, and 0:10 from left to right respectively. (e) Schematic diagram of film morphology with or without coffee-ring (reproduced from ref. [210] with permission from Advanced Materials Technologies).

their light extraction efficiency can be improved. One of the advantages of using EHD printing is that it can print dot patterns in fine sizes. Therefore, the fabrication of microlens arrays by EHD has been investigated for improving the light extraction efficiency of organic LED (OLED) devices in a few studies [205-207]. For instance, Kim and coworkers made gold-coated AgNW films into transparent conductive electrodes, which were then applied to OLED devices [208]. Umbach and coworkers proposed to reduce the effective refractive index by changing the hole transport layer (HTL) and thus improve the output coupling efficiency of OLED [209]. The expectation was achieved through designing electrofluidic spray patterns for morphological ground control of the layers. The layers were nanoporous (78% solid content). The refractive index was reduced by 0.3 and 0.15 in the Zand X/Y directions, respectively. The output coupling efficiency of the OLED was improved by 5-10%. The morphology was maintained by cross-linking hole-transport material, which makes the nanoporous nature of the layer stable over time.

Unlike OLEDs, which can be patterned at high resolution using thermal vapor deposition, quantum dot light-emitting diodes (QLED) are better suited for solution processing. Li and coworkers combined powerful EHD printing and mixed solvent method to use quantum dots (QD), ITO, and aluminum as a light-emitting layer, cathode, and anode, respectively, while ZnO, N,N'-di(1-naphthyl)-N,N'-diphenyl-(1,1'-biphenyl)-4,4'-diamine (NPB), and MoO₃ were selected as electron transport layer, HTL, and hole injection layer to fabricate high-performance QLEDs [210]. The coffee ring was completely suppressed by mixing the solvent toluene and nonane at a ratio of 8:2. A high-resolution QD matrix with a diameter of 1 µm and 306 PPI pixel pits was successfully fabricated. Based on perfect QD films in each pixel pit, inverse pixelated QLEDs with a low on-state voltage of 3 V and a maximum brightness of 8,533 cd/m² at 9 V were obtained. This achievement of high-resolution and highbrightness QLED devices demonstrates the great potential of EHD printing for QD commercial display fabrication (Figure 18).

Zhu and coworkers prepared precursor inks for EHD printing by adding cesium halides (CsBr, CsCl, CsI), lead halides (PbBr₂, PbCl₂, PbI₂), 2-phenylethylamine bromide and a certain proportion of crown ether in dimethyl sulfoxide through a simple solution mixing process for fullcolor, strong emission, and high-resolution display [211]. The colors of displays can be tuned by changing the amount of bromine ions, chloride ions, and iodine ions within the mixture. A high-resolution dot array of less than 5 µm was achieved. Monochromatic and mixed halide fullcolor emission CsPbX3 inks were prepared for chalcogenide.

In a study by Nguyen et al. [212], they calculated an initial QD droplet size, rate of solvent evaporation, and time of flight of electrospray. The layer-by-layer deposition of the final QD droplet showed a surface roughness of 0.0308 µm. The QLED showed a maximum brightness of 12,082 cd/m², a maximum EQE value of 1.86%, and a maximum current efficiency close to 4.0 cd/A. They also pointed out that the EHD electrospray method could be applied to QLEDs and fully printed electronic devices for compatibility, among other advantages.

5 Conclusion and perspectives

This review work discusses the potential challenges and opportunities from the point of view of engineering applications, aiming at providing an overview of the latest developments in EHD printing technology from the perspective of printing and manufacturing processes. Compared with conventional printing, EHD printing is able to avoid contamination of functional materials through non-contact, no mask pattern design, while the materials are sprayed directly onto corresponding coordinates as required. Accordingly, EHD printing principle is clear; with basic processing techniques, it is able to print highly-demanding flexible electronic devices. Due to its specific patterning method, it can be printed on demand by adjusting its process parameters. The deposition volume can be controlled very precisely. However, there are still many challenges that need to be addressed for EHD printing if involving highvolume production prospects. Simultaneous printing using multiple nozzles improves printing rates, but how to improve the printing accuracy becomes a challenge. It is able to meet the needs of multiple-material printing by using multiple nozzles (for different ink materials); however, the printing time has not been significantly reduced. It is believed that arrayproducible, multi-material-convertible EHD printing has greater promise for future applications.

Funding information: This work was financially supported by the Science and Technology Support Plan for Youth Innovation of Colleges in Shandong Province (DC2000000891), the National Natural Science Foundation of China (Grant no. 62104123), the Young Taishan Scholars Program of Shandong Province (No. 201909099), and the National Natural Science Foundation of China (Grant no 52003134).

Author contributions: All authors have accepted responsibility for the entire content of this manuscript and approved its submission.

Conflict of interest: The authors state no conflict of interest.

References

- Li D, Lai WY, Zhang YZ, Huang W. Printable transparent conductive films for flexible electronics. Adv Mater. 2018;30(10):1704738.
- Gao W, Ota H, Kiriya D, Takei K, Javey A. Flexible electronics toward wearable sensing. Acc Chem Res. 2019;52(3):523-33.
- [3] Yang Y. Gao W. Wearable and flexible electronics for continuous molecular monitoring. Chem Soc Rev. 2019;48(6):1465-91.
- [4] Han Y, Dong J. Electrohydrodynamic printing for advanced micro/nanomanufacturing: Current progresses, opportunities, and challenges. J Micro Nano-Manufacturing. 2018;6(4):040802.
- [5] Zhang B, He J, Lei Q, Li D. Electrohydrodynamic printing of sub-microscale fibrous architectures with improved cell adhesion capacity. Virtual Phys Prototyp. 2020;15(1):62-74.
- Gao D, Zhou JG. Designs and applications of electrohydro-[6] dynamic 3D printing. Int J Bioprinting. 2019;5(1):172.
- [7] Galliker P, Schneider J, Eghlidi H, Kress S, Sandoghdar V, Poulikakos D. Direct printing of nanostructures by electrostatic autofocussing of ink nanodroplets. Nat Commun. 2012;3(1):1-9.
- [8] Chen M, Lee H, Yang J, Xu Z, Huang N, Chan BP, et al. Parallel, multi-material electrohydrodynamic 3D nanoprinting. Small. 2020;16(13):1906402.
- [9] Onses MS, Sutanto E, Ferreira PM, Alleyne AG, Rogers JA. Mechanisms, capabilities, and applications of high-resolution electrohydrodynamic jet printing. Small. 2015;11(34):4237-66.
- [10] Cai S, Sun Y, Wang Z, Yang W, Li X, Yu H. Mechanisms, influencing factors, and applications of electrohydrodynamic jet printing. Nanotechnol Rev. 2021;10(1):1046-78.
- Zhang B, He J, Li X, Xu F, Li D. Micro/nanoscale electrohydrodynamic printing: from 2D to 3D. Nanoscale. 2016:8(34):15376-88.
- Cui Z. Printed electronics: materials, technologies and applications. Hoboken, New Jersey, USA: John Wiley & Sons; 2016.
- Aksay IA, Saville DA, Poon HF, Korkut S, Chen C-H. Electrohydrodynamic printing and manufacturing. US Pat, US8906285B2, 2014.
- Alleyne A, Barton K, Mishra S, Ferreira P, Rogers J. High [14] resolution sensing and control of electrohydrodynamic jet printing. US Pat, US8562095B2, 2013.
- [15] Rogers JA, Jang-Ung P, Ferreira PM, Mukhopadhyay D. High resolution electrohydrodynamic jet printing for manufacturing systems. US Pat, US9061494B2, 2015.
- [16] Yin Z, Huang Y, Duan Y, Zhang H. Electrohydrodynamic directwriting for flexible electronic manufacturing. New York City, USA: Springer; 2018.
- [17] Guarino V, Ambrosio L. Electrofluidodynamic technologies (EFDTs) for biomaterials and medical devices: principles and advances. Woodhead Publishing; 2018.
- Ewing J. Thomson's siphon recorder. J Soc Telegr Eng. [18] 1876;5(13):185-212.

- Kavadiya S, Biswas P. Electrospray deposition of biomolecules: Applications, challenges, and recommendations. J Aerosol Sci. 2018;125:182-207.
- [20] Taylor GI. Disintegration of water drops in an electric field. Proc R Soc Lond Ser A Math Phys Sci. 1964;280(1382):383-97.
- [21] Sweet RG. High frequency recording with electrostatically deflected ink jets. Rev Sci Instrum. 1965;36(2):131-6.
- [22] Lewis AM, Brown JAD. Electrically operated character printer. US Pat, US3298030A, 1967.
- [23] Murakami T, Hosaka Y, Nagato H, Hirahara S, Nakao H, Ishii K, et al. Ink-jet recording system using electrostatic force to expel ink. US Pat, US6158844A, 2000.
- [24] Lee D-Y, Shin Y-S, Park S-E, Yu T-U, Hwang J. Electrohydrodynamic printing of silver nanoparticles by using a focused nanocolloid jet. Appl Phys Lett. 2007;90(8):081905.
- [25] Havati I, Bailey A, Tadros TF. Mechanism of stable jet formation in electrohydrodynamic atomization. Nature. 1986;319(6048):41-3.
- Chen C-H, Saville D, Aksay IA. Scaling laws for pulsed elec-[26] trohydrodynamic drop formation. Appl Phys Lett. 2006;89(12):124103.
- [27] Park J-U, Hardy M, Kang SJ, Barton K, Adair K, Mukhopadhyay Dk, et al. High-resolution electrohydrodynamic jet printing. Nat Mater. 2007;6(10):782-9.
- [28] Huang Y, Duan Y, Ding Y, Bu N, Pan Y, Lu N, et al. Versatile, kinetically controlled, high precision electrohydrodynamic writing of micro/nanofibers. Sci Rep. 2014;4(1):5949.
- [29] Liashenko I, Rosell-Llompart J, Cabot A. Ultrafast 3D printing with submicrometer features using electrostatic jet deflection. Nat Commun. 2020;11(1):1-9.
- [30] Su S, Liang J, Wang Z, Xin W, Li X, Wang D. Microtip focused electrohydrodynamic jet printing with nanoscale resolution. Nanoscale. 2020;12(48):24450-62.
- [31] Zhang P, Wang Z, Li J, Li X, Cheng L. From materials to devices using fused deposition modeling: A state-of-art review. Nanotechnol Rev. 2020;9(1):1594-609.
- [32] Kwon H-J, Hong J, Nam SY, Choi HH, Li X, Jeong YJ, et al. Overview of recent progress in electrohydrodynamic jet printing in practical printed electronics: focus on variety of printable materials for each component. Mater Adv. 2021;2:5593-615.
- Kim J, Tran SBQ, Seong B, Lee H, Kang G, Ko JH, et al. Experimental study on fluid selection for a stable Taylor cone formation via micro-PIV measurement. J Vis. 2020;23(3):449-57.
- Jung EM, Lee SW, Kim SH. Printed ion-gel transistor using [34] electrohydrodynamic (EHD) jet printing process. Org Electron. 2018;52:123-9.
- Zhao K, Wang W, Yang Y, Wang K, Yu D-G. From Taylor cone to [35] solid nanofiber in tri-axial electrospinning: Size relationships. Results Phys. 2019;15:102770.
- An S, Lee MW, Kim NY, Lee C, Al-Deyab SS, James SC, et al. [36] Effect of viscosity, electrical conductivity, and surface tension on direct-current-pulsed drop-on-demand electrohydrodynamic printing frequency. Appl Phys Lett. 2014;105(21):214102.
- Onses MS, Sutanto E, Ferreira PM, Alleyne AG, Rogers JA. [37] Mechanisms, capabilities, and applications of high-

- resolution electrohydrodynamic jet printing. Small. 2015;11(34):4237-66.
- [38] Kuang M, Wang L, Song Y. Controllable printing droplets for high-resolution patterns. Adv Mater. 2014;26(40):6950-8.
- Cho TH, Farjam N, Allemang CR, Pannier CP, Kazyak E, Huber C, et al. Area-selective atomic layer deposition patterned by electrohydrodynamic jet printing for additive manufacturing of functional materials and devices. ACS Nano. 2020;14(12):17262-72.
- Véliz B, Bermejo S, Vives J, Castañer L. Large area deposition of ordered nanoparticle layers by electrospray. Colloid Interface Sci Commun. 2018;25:16-21.
- Vass P, Szabó E, Domokos A, Hirsch E, Galata D, Farkas B, et al. Scale-up of electrospinning technology: Applications in the pharmaceutical industry. Wiley Interdiscip Rev Nanomed Nanobiotechnol. 2020;12(4):e1611.
- Rosell-Llompart J, Grifoll J, Loscertales IG. Electrosprays in the cone-jet mode: From Taylor cone formation to spray development. J Aerosol Sci. 2018;125:2-31.
- Wang Z, Chen X, Zeng J, Liang F, Wu P, Wang H. Controllable deposition distance of aligned pattern via dual-nozzle nearfield electrospinning. AIP Adv. 2017;7(3):035310.
- Zhang X, Chi X, Li Z, Yuan Z, Yang J, Zhu L, et al. An electro-[44] hydrodynamic (EHD) printing method with nanosilver ink for flexible electronics. Int J Mod Phys B. 2020;34(17):2050154.
- [45] Wang Z, Wang Q, Zhang Y, Jiang Y, Xia L. Formation of monodispersed droplets with electric periodic dripping regime in electrohydrodynamic (EHD) atomization. Chin J Chem Eng. 2020;28(5):1241-9.
- [46] Phung TH, Kim S, Kwon K-S. A high speed electrohydrodynamic (EHD) jet printing method for line printing. J Micromech Microeng. 2017;27(9):095003.
- Elele E, Shen Y, Boppana R, Afolabi A, Bilgili E, Khusid B. Electro-hydrodynamic drop-on-demand printing of aqueous suspensions of drug nanoparticles. Pharmaceutics. 2020;12(11):1034.
- Lim S, Park SH, An TK, Lee HS, Kim SH. Electrohydrodynamic printing of poly(3,4-ethylenedioxythiophene):poly(4-styrenesulfonate) electrodes with ratio-optimized surfactant. RSC Adv. 2016;6(3):2004-10.
- [49] Li H, Zhu X, Li Z, Yang J, Lan H. Preparation of nano silver paste and applications in transparent electrodes via electricfield driven micro-scale 3D PRINTING. Nanomaterials. 2020;10(1):107.
- Kwon K-S, Rahman MK, Phung TH, Hoath S, Jeong S, Kim JS. Review of digital printing technologies for electronic materials. Flex Print Electron. 2020;6(1):043003.
- [51] Scheideler WJ, Chen C-H. The minimum flow rate scaling of Taylor cone-jets issued from a nozzle. Appl Phys Lett. 2014;104(2):024103.
- He J-H. On the height of Taylor cone in electrospinning. [52] Results Phys. 2020;17:103096.
- Bae J, Lee J, Hyun, Kim S. Effects of polymer properties on [53] jetting performance of electrohydrodynamic printing. J Appl Polym Sci. 2017;134(35):45044.
- Jiang Z, Gan Y, Shi Y. An improved model for prediction of the cone-jet formation in electrospray with the effect of space charge. J Aerosol Sci. 2020;139:105463.

- Wang DZ, Jayasinghe SN, Edirisinghe MJ. High resolution print-patterning of a nano-suspension. J Nanopart Res. 2005;7(2):301-6.
- [56] Rahmanpour M, Ebrahimi R, Pourrajabian A. Numerical simulation of two-phase electrohydrodynamic of stable Taylor cone-jet using a volume-of-fluid approach. J Braz Soc Mech Sci Eng. 2017;39(11):4443-53.
- Collins RT, Sambath K, Harris MT, Basaran OA. Universal [57] scaling laws for the disintegration of electrified drops. Proc Natl Acad Sci. 2013;110(13):4905-10.
- [58] Yu M, Ahn KH, Lee SJ. Design optimization of ink in electrohydrodynamic jet printing: Effect of viscoelasticity on the formation of Taylor cone jet. Mater Des. 2016;89:109-15.
- [59] Wang X, Zheng G, Luo Z, Li W. Current characteristics of various ejection modes in electrohydrodynamic printing. AIP Adv. 2015;5(12):127120.
- [60] Zou W, Yu H, Zhou P, Liu L. Tip-assisted electrohydrodynamic jet printing for high-resolution microdroplet deposition. Mater Des. 2019;166:107609.
- [61] Li Z, Al-Milaji KN, Zhao H, Chen D-R. Electrohydrodynamic (EHD) jet printing with a circulating dual-channel nozzle. J Micromech Microeng. 2019;29(3):035013.
- Qin H, Wei C, Dong J, Lee Y-S. Direct printing and electrical [62] characterization of conductive micro-silver tracks by alternating current-pulse modulated electrohydrodynamic jet printing. J Manuf Sci Eng. 2016;139:2.
- [63] Wu S, Ahmad Z, Li J-S, Chang M-W. Fabrication of flexible composite drug films via foldable linkages using electrohydrodynamic printing. Mater Sci Eng C. 2020;108:110393.
- [64] Fang F, Tao X, Chen X, Wang H, Wu P, Zhang J, et al. Microlens fabrication by replica molding of electro-hydrodynamic printing liquid mold. Micromachines. 2020;11(2):161.
- Fujii M, Kobayashi N, Koeda H, Miyashita I, Oguchi A, Sugimura S. Ink jet printer having an electrostatic activator and its control method. US Pat, US5821951A, 1998.
- [66] Wang X, Xu L, Zheng G, Cheng W, Sun D. Pulsed electrohydrodynamic printing of conductive silver patterns on demand. Sci China Technol Sci. 2012;55(6):1603-7.
- [67] Kwon K-S, Lee D-Y. Investigation of pulse voltage shape effects on electrohydrodynamic jets using a vision measurement technique. J Micromech Microeng. 2013;23(6):065018.
- [68] Juraschek R, Röllgen FW. Pulsation phenomena during electrospray ionization. Int J Mass Spectrometry. 1998;177(1):1-15.
- Kim J, Oh H, Kim SS. Electrohydrodynamic drop-on-demand patterning in pulsed cone-jet mode at various frequencies. J Aerosol Sci. 2008;39(9):819-25.
- [70] Wu C, Tetik H, Cheng J, Ding W, Guo H, Tao X, et al. Electrohydrodynamic jet printing driven by a triboelectric nanogenerator. Adv Funct Mater. 2019;29(22):1901102.
- Xu L, Wang X, Huang Y, Sun D, Lin L, editors. Jetting frequency [71] vs voltage frequency in the low-frequency pulsation mode of electrohydrodynamic printing. 2010 IEEE 5th International Conference on Nano/Micro Engineered and Molecular Systems; 2010, 20-23 Jan.
- [72] Choi HK, Park J-U, Park OO, Ferreira PM, Georgiadis JG, Rogers JA. Scaling laws for jet pulsations associated with high-resolution electrohydrodynamic printing. Appl Phys Lett. 2008;92(12):123109.

- [73] Lee M, Kang D, Kim N, Kim HY, James S, Yoon S. A study of ejection modes for pulsed-DC electrohydrodynamic inkjet printing. J Aerosol Sci. 2012;46:1-6.
- [74] Wei C, Qin H, Chiu C-P, Lee Y-S, Dong J. Drop-on-demand Ejet printing of continuous interconnects with AC-pulse modulation on highly insulating substrates. J Manuf Syst. 2015;37:505-10.
- Wei C, Qin H, Ramírez-Iglesias NA, Chiu C-P, Lee Y-S, Dong J. [75] High-resolution ac-pulse modulated electrohydrodynamic jet printing on highly insulating substrates. J Micromech Microeng. 2014;24(4):045010.
- Taglioli M, Shaw A, Wright A, Fitzpatrick B, Neretti G, Seri P, et al. EHD-driven mass transport enhancement in surface dielectric barrier discharges. Plasma Sources Sci Technol. 2016;25(6):06LT1.
- Mishra S, Barton KL, Alleyne AG, Ferreira PM, Rogers JA. High-speed and drop-on-demand printing with a pulsed electrohydrodynamic jet. J Micromech Microeng. 2010;20(9):095026.
- [78] Kim Y, Jang S, Oh JH. High-resolution electrohydrodynamic printing of silver nanoparticle ink via commercial hypodermic needles. Appl Phys Lett. 2015;106(1):014103.
- Barton K, Mishra S, Alleyne A, Ferreira P, Rogers J. Control of [79] high-resolution electrohydrodynamic jet printing. Control Eng Pract. 2011;19(11):1266-73.
- Jang Y, Hartarto Tambunan I, Tak H, Dat Nguyen V, Kang T, Byun D. Non-contact printing of high aspect ratio Ag electrodes for polycrystalline silicone solar cell with electrohydrodynamic jet printing. Appl Phys Lett. 2013;102(12):123901.
- [81] Schneider J, Rohner P, Thureja D, Schmid M, Galliker P, Poulikakos D. Electrohydrodynamic nanodrip printing of high aspect ratio metal grid transparent electrodes. Adv Funct Mater. 2016;26(6):833-40.
- [82] Reiser A, Lindén M, Rohner P, Marchand A, Galinski H, Sologubenko AS, et al. Multi-metal electrohydrodynamic redox 3D printing at the submicron scale. Nat Commun.
- Zong H, Xia X, Liang Y, Dai S, Alsaedi A, Hayat T, et al. Designing function-oriented artificial nanomaterials and membranes via electrospinning and electrospraying techniques. Mater Sci Eng C. 2018;92:1075-91.
- [84] Yu DG, Wang M, Li X, Liu X, Zhu LM, Annie Bligh SW. Multifluid electrospinning for the generation of complex nanostructures. Wiley Interdiscip Rev Nanomed Nanobiotechnol. 2020;12(3):e1601.
- Xue J, Wu T, Dai Y, Xia Y. Electrospinning and electrospun [85] nanofibers: Methods, materials, and applications. Chem Rev. 2019;119(8):5298-415.
- Huang Y, Bu N, Duan Y, Pan Y, Liu H, Yin Z, et al. Electrohydrodynamic direct-writing. Nanoscale. 2013;5(24):12007-17.
- [87] Reneker DH, Yarin AL. Electrospinning jets and polymer nanofibers. Polymer. 2008;49(10):2387-425.
- [88] Lu T, Cui J, Qu Q, Wang Y, Zhang J, Xiong R, et al. Multistructured electrospun nanofibers for air filtration: a review. ACS Appl Mater Interfaces. 2021;13(20):23293-313.
- Yoon J, Yang HS, Lee BS, Yu WR. Recent progress in coaxial electrospinning: New parameters, various structures, and wide applications. Adv Mater. 2018;30(42):1704765.

- Huang C-Y, Chiu C-W. Facile fabrication of a stretchable and flexible nanofiber carbon film-sensing electrode by electrospinning and its application in smart clothing for ECG and EMG monitoring. ACS Appl Electron Mater. 2021;3(2):676-86.
- [91] Nazemi MM, Khodabandeh A, Hadjizadeh A. Near-Field Electrospinning: Crucial Parameters, Challenges, and Applications. ACS Appl Bio Mater. 2022;5(2):394-412.
- [92] Shin D, Kim J, Chang J. Experimental study on jet impact speed in near-field electrospinning for precise patterning of nanofiber. J Manuf Process. 2018;36:231-7.
- [93] Shin D, Choi S, Kim J, Regmi A, Chang J. Direct-printing of functional nanofibers on 3D surfaces using self-aligning nanojet in near-field electrospinning. Adv Mater Technol. 2020;5(6):2000232.
- [94] Lim L-T, Mendes AC, Chronakis IS. Electrospinning and electrospraying technologies for food applications. Adv food Nutr Res. 2019;88:167-234.
- [95] Bodnár E, Grifoll J, Rosell-Llompart J. Polymer solution electrospraying: A tool for engineering particles and films with controlled morphology. J Aerosol Sci. 2018;125:93-118.
- [96] Reneker DH, Yarin AL, Fong H, Koombhongse S. Bending instability of electrically charged liquid jets of polymer solutions in electrospinning. J Appl Phys. 2000;87(9):4531-47.
- [97] Buchko CJ, Chen LC, Shen Y, Martin DC. Processing and microstructural characterization of porous biocompatible protein polymer thin films. Polymer. 1999;40(26):7397-407.
- [98] Wang Y, Hashimoto T, Li CC, Li YC, Wang C. Extension rate of the straight jet in electrospinning of poly (N-isopropyl acrylamide) solutions in dimethylformamide: Influences of flow rate and applied voltage. J Polym Sci Part B Polym Phys. 2018;56(4):319-29.
- He Z, Rault F, Lewandowski M, Mohsenzadeh E, Salaün F. Electrospun PVDF nanofibers for piezoelectric applications: A review of the influence of electrospinning parameters on the β phase and crystallinity enhancement. Polymers. 2021;13(2):174.
- [100] Sener AG, Altay AS, Altay F, editors. Effect of voltage on morphology of electrospun nanofibers. 2011 7th International Conference on Electrical and Electronics Engineering (ELECO). IEEE; 2011.
- [101] Jiyong H, Yinda Z, Hele Z, Yuanyuan G, Xudong Y. Mixed effect of main electrospinning parameters on the β-phase crystallinity of electrospun PVDF nanofibers. Smart Mater Struct. 2017;26(8):085019.
- [102] Großhaus C, Bakirci E, Berthel M, Hrynevich A, Kade JC, Hochleitner G, et al. Melt electrospinning of nanofibers from medical-grade poly ($\epsilon\textsc{-}\mathsf{Caprolactone})$ with a modified nozzle. Small. 2020;16(44):2003471.
- [103] Vicente A, Rivero PJ, Palacio JF, Rodríguez R. The role of the fiber/bead hierarchical microstructure on the properties of PVDF coatings deposited by electrospinning. Polymers. 2021;13(3):464.
- [104] Singh RK, Lye SW, Miao J. Holistic investigation of the electrospinning parameters for high percentage of β-phase in PVDF nanofibers. Polymer. 2021;214:123366.
- [105] Yuan X, Zhang Y, Dong C, Sheng J. Morphology of ultrafine polysulfone fibers prepared by electrospinning. Polym Int. 2004;53(11):1704-10.

- [106] Zargham S, Bazgir S, Tavakoli A, Rashidi AS, Damerchely R. The effect of flow rate on morphology and deposition area of electrospun nylon 6 nanofiber. J Eng Fibers Fabr. 2012;7(4):155892501200700414.
- [107] Gee S, Johnson B, Smith A. Optimizing electrospinning parameters for piezoelectric PVDF nanofiber membranes. J Membr Sci. 2018;563:804-12.
- [108] Wang W, Stipp PN, Ouaras K, Fathi S, Huang YYS. Broad bandwidth, self-powered acoustic sensor created by dynamic near-field electrospinning of suspended, transparent piezoelectric nanofiber mesh. Small. 2020;16(28):2000581.
- [109] Lee TH, Chen CY, Tsai CY, Fuh YK. Near-field electrospun piezoelectric fibers as sound-sensing elements. Polymers. 2018:10(7):692.
- [110] Wong D, Abuzalat O, Ko J, Lee J, Kim S, Park SS. Intense pulsed light-treated near-field electrospun nanofiber on a quartz tuning fork for multimodal gas sensors. ACS Appl Mater Interfaces. 2020;12(21):24308-18.
- [111] Brown TD, Dalton PD, Hutmacher DW. Direct writing by way of melt electrospinning. Adv Mater. 2011;23(47):5651-7.
- [112] Bisht GS, Canton G, Mirsepassi A, Kulinsky L, Oh S, Dunn-Rankin D, et al. Controlled continuous patterning of polymeric nanofibers on three-dimensional substrates using lowvoltage near-field electrospinning. Nano Lett. 2011;11(4):1831-7.
- [113] Kang J, Jang Y, Kim Y, Cho S-H, Suhr J, Hong BH, et al. An Aggrid/graphene hybrid structure for large-scale, transparent, flexible heaters. Nanoscale. 2015;7(15):6567-73.
- [114] Zhang J, Geng B, Duan S, Huang C, Xi Y, Mu Q, et al. Highresolution organic field-effect transistors manufactured by electrohydrodynamic inkjet printing of doped electrodes. J Mater Chem C. 2020;8(43):15219-23.
- [115] Lee Y, Jin W-Y, Cho KY, Kang J-W, Kim J. Thermal pressing of a metal-grid transparent electrode into a plastic substrate for flexible electronic devices. J Mater Chem C. 2016;4(32):7577-83.
- [116] Khalid MAU, Kim SW, Lee J, Soomro AM, Rehman MM, Lee B-G, et al. Resistive switching device based on SrTiO₃/PVA hybrid composite thin film as active layer. Polymer. 2020:189:122183.
- [117] Alzakia FI, Jonhson W, Ding J, Tan SC. Ultrafast exfoliation of 2D materials by solvent activation and one-step fabrication of all-2D-material photodetectors by electrohydrodynamic printing. ACS Appl Mater Interfaces. 2020;12(25):28840-51.
- [118] Layani M, Kamyshny A, Magdassi S. Transparent conductors composed of nanomaterials. Nanoscale. 2014;6(11):5581-91.
- Reiser A, Lindén M, Rohner P, Marchand A, Galinski H, [119] Sologubenko AS, et al. Multi-metal electrohydrodynamic redox 3D printing at the submicron scale. Nat Commun. 2019;10(1):1853.
- [120] Jafry AT, Lee H, Tenggara AP, Lim H, Moon Y, Kim S-H, et al. Double-sided electrohydrodynamic jet printing of twodimensional electrode array in paper-based digital microfluidics. Sens Actuators B Chem. 2019;282:831-7.
- [121] Wu X, Zhou Z, Wang Y, Li J. Syntheses of silver nanowires ink and printable flexible transparent conductive film: a review. Coatings. 2020;10(9):865.
- [122] Hoeng F, Denneulin A, Reverdy-Bruas N, Krosnicki G, Bras J. Rheology of cellulose nanofibrils/silver nanowires

- suspension for the production of transparent and conductive electrodes by screen printing. Appl Surf Sci. 2017;394:160-8.
- [123] Xu J, Guo H, Ding H, Wang Q, Tang Z, Li Z, et al. Printable and recyclable conductive ink based on a liquid metal with excellent surface wettability for flexible electronics. ACS Appl Mater Interfaces. 2021;13(6):7443-52.
- [124] Wang B, Chen X, Ahmad Z, Huang J, Chang M-W. 3D electrohydrodynamic printing of highly aligned dual-core graphene composite matrices. Carbon. 2019;153:285-97.
- [125] Kunpai C, Kang MG, Song H-E, Shin D-Y. Fine front side metallisation by stretching the dispensed silver paste filament with graphite nanofibres. Sol Energy Mater Sol Cell. 2017:169:167-76.
- [126] Jeong YJ, Bae J, Nam S, Lim S, Jang J, Kim SH, et al. Directly drawn ZnO semiconductors and MWCNT/PSS electrodes via electrohydrodynamic jet printing for use in thin-film transistors: The ideal combination for reliable device performances. Org Electron. 2016;39:272-8.
- [127] Niaraki Asli AE, Guo J, Lai PL, Montazami R, Hashemi NN. High-yield production of aqueous graphene for electrohydrodynamic drop-on-demand printing of biocompatible conductive patterns. Biosensors. 2020;10(1):6.
- [128] Grotevent MJ, Hail CU, Yakunin S, Dirin DN, Thodkar K, Borin Barin G, et al. Nanoprinted quantum dot-graphene photodetectors. Adv Optical Mater. 2019;7(11):1900019.
- [129] Xu W, Zhang S, Xu W. Recent progress on electrohydrodynamic nanowire printing. Sci China Mater. 2019;62(11):1709-26.
- [130] Meng Z, He J, Xia Z, Li D. Fabrication of microfibrous PCL/ MWCNTs scaffolds via melt-based electrohydrodynamic printing. Mater Lett. 2020;278:128440.
- [131] Liu J, Xiao L, Rao Z, Dong B, Yin Z, Huang Y. High-performance, micrometer thick/conformal, transparent metal-network electrodes for flexible and curved electronic devices. Adv Mater Technol. 2018;3(8):1800155.
- [132] Coppola S, Mecozzi L, Vespini V, Battista L, Grilli S, Nenna G, et al. Nanocomposite polymer carbon-black coating for triggering pyro-electrohydrodynamic inkjet printing. Appl Phys Lett. 2015:106(26):261603.
- [133] Liu X, Paquet C, Malenfant PRL, Deore B. Silver molecular ink with low viscosity and low processing temperature. US Pat, US20190375958A1, 2019.
- [134] Yang W, List-Kratochvil EJ, Wang C. Metal particle-free inks for printed flexible electronics. J Mater Chem C. 2019;7(48):15098-117.
- [135] Liu G, Yang W, Wang C, Rao J. A rapid fabrication approach for the capacitive accelerometer based on 3D printing and a silver particle-free ink. J Mater Sci Mater Electron. 2021;32:17901-10.
- [136] Can TTT, Nguyen TC, Choi W-S. Patterning of high-viscosity silver paste by an electrohydrodynamic-Jet printer for use in TFT applications. Sci Rep. 2019;9(1):1-8.
- $[137] \quad \text{Han Y, Dong J. Electrohydrodynamic (EHD) printing of molten} \\$ metal ink for flexible and stretchable conductor with selfhealing capability. Adv Mater Technol. 2018;3(3):1700268.
- [138] Lee SH, Jun B-H. Silver nanoparticles: synthesis and application for nanomedicine. Int J Mol Sci. 2019;20(4):865.
- [139] Chou Chao C-T, Chou Chau Y-F, Huang HJ, Kumara N, Kooh MRR, Lim CM, et al. Highly sensitive and tunable

- plasmonic sensor based on a nanoring resonator with silver nanorods. Nanomaterials. 2020;10(7):1399.
- [140] Lee H, Jang H-S, Cho D-H, Lee J, Seong B, Kang G, et al. Redox-active tyrosine-mediated peptide template for largescale single-crystalline two-dimensional silver nanosheets. ACS nano. 2020;14(2):1738-44.
- [141] Zhang P, Wyman I, Hu J, Lin S, Zhong Z, Tu Y, et al. Silver nanowires: Synthesis technologies, growth mechanism and multifunctional applications. Mater Sci Eng B. 2017;223:1-23.
- [142] Zhang Z, Shen W, Xue J, Liu Y, Liu Y, Yan P, et al. Recent advances in synthetic methods and applications of silver nanostructures. Nanoscale Res Lett. 2018;13(1):1-18.
- [143] Li X, Park H, Lee MH, Hwang B, Kim SH, Lim S. High resolution patterning of Ag nanowire flexible transparent electrode via electrohydrodynamic jet printing of acrylic polymer-silicate nanoparticle composite overcoating layer. Org Electron. 2018;62:400-6.
- [144] Jin C, Liu C, Liu X, Wang Y, Hwang H. Experimental and simulation study on BCTZ-based flexible energy harvesting device filled with Ag-coated Cu particles. Ceram Int. 2018;44(14):17391-8.
- [145] Lee C, Kim NR, Koo J, Lee YJ, Lee HM. Cu-Ag core-shell nanoparticles with enhanced oxidation stability for printed electronics. Nanotechnology. 2015;26(45):455601.
- Nie X, Wang H, Zou J. Inkjet printing of silver citrate conductive ink on PET substrate. Appl Surf Sci. 2012;261:554-60.
- [147] Kell AJ, Paquet C, Mozenson O, Djavani-Tabrizi I, Deore B, Liu X, et al. Versatile molecular silver ink platform for printed flexible electronics. ACS Appl Mater interfaces. 2017;9(20):17226-37.
- [148] Navaladian S, Viswanathan B, Viswanath R, Varadarajan T. Thermal decomposition as route for silver nanoparticles. Nanoscale Res Lett. 2007;2(1):44-8.
- [149] Bhat KS, Nakate UT, Yoo J-Y, Wang Y, Mahmoudi T, Hahn Y-B. Cost-effective silver ink for printable and flexible electronics with robust mechanical performance. Chem Eng J. 2019;373:355-64.
- [150] Vaseem M, McKerricher G, Shamim A. Robust design of a particle-free silver-organo-complex ink with high conductivity and inkjet stability for flexible electronics. ACS Appl Mater interfaces. 2016;8(1):177-86.
- [151] Manjunath G, Pujar P, Gupta B, Gupta D, Mandal S. Lowtemperature reducible particle-free screen-printable silver ink for the fabrication of high conductive electrodes. J Mater Sci Mater Electron. 2019;30(20):18647-58.
- [152] Dong Y, Li X, Liu S, Zhu Q, Zhang M, Li J-G, et al. Optimizing formulations of silver organic decomposition ink for producing highly-conductive features on flexible substrates: The case study of amines. Thin Solid Films. 2016;616:635-42.
- [153] Lei Q, He J, Zhang B, Chang J, Li D. Microscale electrohydrodynamic printing of conductive silver features based on in situ reactive inks. J Mater Chem C. 2018;6(2):213-8.
- [154] Zope KR, Cormier D, Williams SA. Reactive silver oxalate ink composition with enhanced curing conditions for flexible substrates. ACS Appl Mater interfaces. 2018;10(4):3830-7.
- [155] Iijima S. Helical microtubules of graphitic carbon. nature. 1991;354(6348):56-8.

- [156] Hwang H-J, Joo S-J, Kim H-S. Copper nanoparticle/multiwalled carbon nanotube composite films with high electrical conductivity and fatigue resistance fabricated via flash light sintering. ACS Appl Mater interfaces. 2015;7(45):25413-23.
- [157] Jeong YJ, Lee X, Bae J, Jang J, Joo SW, Lim S, et al. Direct patterning of conductive carbon nanotube/polystyrene sulfonate composites via electrohydrodynamic jet printing for use in organic field-effect transistors. J Mater Chem C. 2016;4(22):4912-9.
- [158] Bai J, Zhong X, Jiang S, Huang Y, Duan X. Graphene nanomesh. Nat Nanotechnol. 2010;5(3):190-4.
- [159] Garcia de Abajo FJ. Graphene plasmonics: challenges and opportunities. Acs Photonics. 2014;1(3):135-52.
- [160] Tiwari SK, Sahoo S, Wang N, Huczko A. Graphene research and their outputs: Status and prospect. J Sci Adv Mater Devices. 2020;5(1):10-29.
- [161] Ali S, Bae J, Lee CH. Stretchable photo sensor using perylene/graphene composite on ridged polydimethylsiloxane substrate. Opt Exp. 2015;23(24):30583-91.
- [162] Hwang B, Li X, Kim SH, Lim S. Effect of carbon nanotube addition on mechanical reliability of Ag nanowire network. Mater Lett. 2017;198:202-5.
- [163] Chang J, He J, Lei Q, Li D. Electrohydrodynamic printing of microscale PEDOT: PSS-PEO features with tunable conductive/thermal properties. ACS Appl Mater interfaces. 2018;10(22):19116-22.
- [164] Eduok U, Faye O, Szpunar J. Recent developments and applications of protective silicone coatings: A review of PDMS functional materials. Prog Org Coat. 2017;111:124-63.
- [165] Vijayavenkataraman S, Thaharah S, Zhang S, Lu WF, Fuh JYH. Electrohydrodynamic jet 3D-printed PCL/PAA conductive scaffolds with tunable biodegradability as nerve guide conduits (NGCs) for peripheral nerve injury repair. Mater Des. 2019:162:171-84.
- [166] Jiang L, Huang Y, Zhang X, Qin H. Electrohydrodynamic inkjet printing of Polydimethylsiloxane (PDMS). Procedia Manuf. 2020;48:90-4.
- Shao F, Wan Q. Recent progress on jet printing of oxide-[167] based thin film transistors. J Phys D Appl Phys. 2019:52(14):143002.
- [168] Chen K, Chou W, Liu L, Cui Y, Xue P, Jia M. Electrochemical sensors fabricated by electrospinning technology: An overview. Sensors. 2019;19(17):3676.
- [169] He J, Zhang B, Li Z, Mao M, Li J, Han K, et al. High-resolution electrohydrodynamic bioprinting: a new biofabrication strategy for biomimetic micro/nanoscale architectures and living tissue constructs. Biofabrication. 2020;12(4):042002.
- [170] Duan Y, Li H, Yang W, Shao Z, Wang Q, Huang Y, et al. Modetunable, micro/nanoscale electrohydrodynamic deposition techniques for optoelectronic devices fabrication. Nanoscale. 2022;14:13452-72.
- [171] Kim SJ, Yoon S, Kim HJ. Review of solution-processed oxide thin-film transistors. Jap J Appl Phys. 2014:53;02BA-2S.
- [172] Kim S-Y, Kim K, Hwang Y, Park J, Jang J, Nam Y, et al. Highresolution electrohydrodynamic inkjet printing of stretchable metal oxide semiconductor transistors with high performance. Nanoscale. 2016;8(39):17113-21.
- Kwon Hj YeH, Baek Y, Hong J, Wang R, Choi Y, et al. Printable ultra-flexible fluorinated organic-inorganic nanohybrid

- sol-gel derived gate dielectrics for highly stable organic thin-film transistors and other practical applications. Adv Funct Mater. 2021;31(10):2009539.
- [174] Wu M, Hou S, Yu X, Yu J. Recent progress in chemical gas sensors based on organic thin film transistors. J Mater Chem C. 2020;8(39):13482-500.
- [175] Tang X, Kwon H-J, Ye H, Kim JY, Lee J, Jeong YJ, et al. Enhanced solvent resistance and electrical performance of electrohydrodynamic jet printed PEDOT: PSS composite patterns: effects of hardeners on the performance of organic thin-film transistors. Phys Chem Chem Phys. 2019;21(46):25690-9.
- [176] Kim K, Kim SH, Cheon H, Tang X, Oh JH, Jhon H, et al. Electrohydrodynamic-jet (EHD)-printed diketopyrrolopyroole-based copolymer for OFETs and circuit applications. Polymers. 2019;11(11):1759.
- [177] Can TTT, Ko H-L, Choi W-S. EHD-jet patterned MoS2 on a high-k dielectric for high mobility in thin film transistor applications. Nanotechnology. 2021;32(24):245710.
- [178] Liang Y, Yong J, Yu Y, Nirmalathas A, Ganesan K, Evans R, et al. Direct electrohydrodynamic patterning of high-performance all metal oxide thin-film electronics. ACS nano. 2019;13(12):13957-64.
- [179] Yong J, Liang Y, Yu Y, Hassan B, Hossain MS, Ganesan K, et al. Fully solution-processed transparent artificial neural network using drop-on-demand electrohydrodynamic printing. ACS Appl Mater Interfaces. 2019;11(19):17521-30.
- [180] Han ST, Peng H, Sun Q, Venkatesh S, Chung KS, Lau SC, et al. An overview of the development of flexible sensors. Adv Mater. 2017;29(33):1700375.
- [181] Xuan W, He X, Chen J, Wang W, Wang X, Xu Y, et al. High sensitivity flexible Lamb-wave humidity sensors with a graphene oxide sensing layer. Nanoscale. 2015;7(16):7430-6.
- [182] Kuzubasoglu BA, Bahadir SK. Flexible temperature sensors: A review. Sens Actuators A Phys. 2020;315:112282.
- [183] Wang T, Guo Y, Wan P, Zhang H, Chen X, Sun X. Flexible transparent electronic gas sensors. Small. 2016;12(28):3748-56.
- [184] Zhao L, Qiang F, Dai S-W, Shen S-C, Huang Y-Z, Huang N-J, et al. Construction of sandwich-like porous structure of graphene-coated foam composites for ultrasensitive and flexible pressure sensors. Nanoscale. 2019;11(21):10229-38.
- [185] Liu H, Li Q, Zhang S, Yin R, Liu X, He Y, et al. Electrically conductive polymer composites for smart flexible strain sensors: a critical review. J Mater Chem C. 2018;6(45):12121-41.
- [186] Sturm H, Lang W. Membrane-based thermal flow sensors on flexible substrates. Sens Actuators A Phys. 2013;195:113-22.
- [187] Ahmad S, Rahman K, Shakeel M, Qasuria TAK, Cheema TA, Khan A. A low-cost printed humidity sensor on cellulose substrate by EHD printing. J Mater Res. 2021;36:3667-78.
- [188] Yousaf HZ, Kim SW, Hassan G, Karimov K, Choi KH, Sajid M. Highly sensitive wide range linear integrated temperature compensated humidity sensors fabricated using Electrohydrodynamic printing and electrospray deposition. Sens Actuators B Chem. 2020;308:127680.
- [189] Ali S, Hassan A, Hassan G, Bae J, Lee CH. All-printed humidity sensor based on graphene/methyl-red composite with high sensitivity. Carbon. 2016;105:23-32.
- [190] Jin ML, Park S, Kweon H, Koh HJ, Gao M, Tang C, et al. Scalable Superior Chemical Sensing Performance of

- Stretchable Ionotronic Skin via a π -Hole Receptor Effect. Adv Mater. 2021;33(13):2007605.
- [191] Kang K, Yang D, Park J, Kim S, Cho I, Yang H-H, et al. Micropatterning of metal oxide nanofibers by electrohydrodynamic (EHD) printing towards highly integrated and multiplexed gas sensor applications. Sens Actuators B Chem. 2017;250:574-83.
- [192] Qin H, Cai Y, Dong J, Lee Y-S. Direct printing of capacitive touch sensors on flexible substrates by additive E-jet printing with silver nanoinks. J Manuf Sci Eng. 2017;139(3):031011.
- [193] Zhang B, Seong B, Lee J, Nguyen V, Cho D, Byun D. One-step sub-micrometer-scale electrohydrodynamic inkjet threedimensional printing technique with spontaneous nanoscale joule heating. ACS Appl Mater Interfaces. 2017;9(35):29965-72.
- [194] Liu Z, Li H, Shi B, Fan Y, Wang ZL, Li Z. Wearable and implantable triboelectric nanogenerators. Adv Funct Mater. 2019;29(20):1808820.
- [195] Zhao L, Li H, Meng J, Li Z. The recent advances in self-powered medical information sensors. InfoMat. 2020;2(1):212-34.
- [196] Lou Z, Li L, Wang L, Shen G. Recent progress of self-powered sensing systems for wearable electronics. Small. 2017;13(45):1701791.
- [197] Go E-B, Kim H-T, Kim C-Y. Synthesis of one-dimensional pillar arrays by electrohydrodynamic jet printing for glucose sensor. J Biomed Nanotechnol. 2017;13(1):61-7.
- [198] Pruvost M, Smit WJ, Monteux C, Poulin P, Colin A. Polymeric foams for flexible and highly sensitive low-pressure capacitive sensors. NPJ Flexible Electronics. 2019;3(1):7.
- [199] Nayeem MOG, Lee S, Jin H, Matsuhisa N, Jinno H, Miyamoto A, et al. All-nanofiber-based, ultrasensitive, gaspermeable mechanoacoustic sensors for continuous longterm heart monitoring. Proc Natl Acad Sci. 2020;117(13):7063-70.
- [200] Hwang B-U, Lee J-H, Trung TQ, Roh E, Kim D-I, Kim S-W, et al. Transparent Stretchable Self-Powered Patchable Sensor Platform with Ultrasensitive Recognition of Human Activities. ACS Nano. 2015;9(9):8801-10.
- [201] Yeo M, Kim G. Electrohydrodynamic-direct-printed cell-laden microfibrous structure using alginate-based bioink for effective myotube formation. Carbohydr Polym. 2021;272:118444.
- [202] Wu Y. Electrohydrodynamic jet 3D printing in biomedical applications. Acta Biomaterialia. 2021;128:21-41.
- [203] He J, Xu F, Dong R, Guo B, Li D. Electrohydrodynamic 3D printing of microscale poly (ε-caprolactone) scaffolds with multi-walled carbon nanotubes. Biofabrication. 2017;9(1):015007.
- Jing L, Wang X, Liu H, Lu Y, Bian J, Sun J, et al. Zein increases the cytoaffinity and biodegradability of scaffolds 3D-printed with zein and poly (ε-caprolactone) composite ink. ACS Appl Mater interfaces. 2018;10(22):18551-9.
- [205] Li H, Duan Y, Shao Z, Zhang W, Li H, Yang W, et al. Morphology-programmable self-aligned microlens array for light extraction via electrohydrodynamic printing. Org Electron. 2020;87:105969.
- [206] Mu L, Jiang C, Wang J, Zheng H, Ying L, Xu M, et al. 34-3: OLED display with high resolution fabricated by

- electrohydrodynamic printing. SID Symposium Dig Technical Pap. 2020;51(1):485-8.
- [207] Lee J, Li X, Park J. Fine stripe coating and micro patterning of organic thin films using double nozzles for OLEDs. Org Electron. 2020;87:105957.
- [208] Kim S, Kim B, Im I, Kim D, Lee H, Nam J, et al. Employment of gold-coated silver nanowires as transparent conductive electrode for organic light emitting diodes. Nanotechnology. 2017;28(34):345201.
- [209] Umbach TE, Röllgen S, Schneider S, Klesper H, Umbach AM, Meerholz K. Low-refractive index layers in organic light-emitting diodes via electrospray deposition for enhanced outcoupling efficiencies. Adv Eng Mater. 2020;22(5):1900897.
- [210] Li H, Duan Y, Shao Z, Zhang G, Li H, Huang Y, et al. High-resolution pixelated light emitting diodes based on electrohydrodynamic printing and coffee-ring-free quantum dot film. Adv Mater Technol. 2020;5(10):2000401.
- [211] Zhu M, Duan Y, Liu N, Li H, Li J, Du P, et al. Electrohydrodynamically printed high-resolution full-color hybrid perovskites. Adv Funct Mater. 2019;29(35):1903294.
- [212] Nguyen TC, Choi W-S. Electrospray mechanism for quantum dot thin-film formation using an electrohydrodynamic jet and light-emitting device application. Sci Rep. 2020;10(1):11075.